Available online at www.sciencedirect.com
SCIENCE DIRECT®
ELSEVIER
Mechatronics 14 (2004) 907–945
MECHATRONICS

A review of atomic force microscopy imaging systems: application to molecular metrology and biological sciences

Nader Jalili *, Karthik Laxminarayana

Smart Structures and Nanoelectromechanical Systems Laboratory,
Department of Mechanical Engineering,
Clemson University, Clemson, SC 29634-0921, USA

Accepted 27 April 2004

Abstract

The atomic force microscope (AFM) system has evolved into a useful tool for direct measurements of micro-structural parameters and unraveling the intermolecular forces at nanoscale level with atomic-resolution characterization. Typically, these micro-cantilever systems are operated in three open-loop modes; non-contact mode, contact mode, and tapping mode. In order to probe electric, magnetic, and/or atomic forces of a selected sample, the non-contact mode is utilized by moving the cantilever slightly away from the sample surface and oscillating the cantilever at or near its natural resonance frequency. Alternatively, the contact mode acquires sample attributes by monitoring interaction forces while the cantilever tip remains in contact with the target sample. The tapping mode of operation combines qualities of both the contact and non-contact modes by gleaning sample data and oscillating the cantilever tip at or near its natural resonance frequency while allowing the cantilever tip to impact the target sample for a minimal amount of time. Recent research on AFM systems has focused on many manufacturing and metrology processes at molecular levels due to its tremendous surface microscopic capabilities. This paper provides a review of such recent developments in AFM imaging system with emphasis on operational modes, micro-cantilever dynamic modeling and control. Due to the important contributions of AFM systems to metrology and biological sciences, this study also provides a comprehensive review of recent applications of different AFM systems in these two important areas.

* Corresponding author. Tel.: +1-864-656-5642; fax: +1-864-656-4435.
E-mail address: jalili@clemson.edu (N. Jalili).

0957-4158/$ - see front matter © 2004 Elsevier Ltd. All rights reserved.
doi:10.1016/j.mechatronics.2004.04.005

1. Introduction

The atomic force microscope (AFM) system has evolved into a useful tool for direct measurements of intermolecular forces with atomic-resolution characterization that can be employed in a broad spectrum of applications such as electronics, semi-conductors, materials and manufacturing, polymers, biology and biomaterials. AFM provides additional capabilities and advantages relative to other microscopic methods (e.g. scanning electron microscopy (SEM) and transmission electron microscopy (TEM)) in studies of metallic surfaces and micro-structures by providing reliable measurements at the nanometer scale [37,57,75,121,123]. AFM can also be used for nanoindentation to provide *in situ* imaging ability without moving the sample, switching tips, relocating the area for scanning, or using an entirely different instrument to image the indentation [35,56,71,102,118]. Force modulation microscopy (FMM) which is an extension of AFM imaging, is used extensively for the characterization of mechanical properties and in applications such as imaging composition changes in a composite material, analyzing polymer homogeneity, and detecting contaminants in manufacturing processes [3,27,99]. Assembly of nanoparticles and linking them to electrical leads, such as random deposition of clusters between electrodes, binding by wet chemistry, and electrostatic trapping, all serve as other important applications of the AFM technique.

As depicted in Fig. 1, a typical AFM system consists of a micro-machined cantilever probe and a sharp tip mounted to a Piezoelectric (PZT) actuator and a position sensitive photo detector for receiving a laser beam reflected off the end-point of the beam to provide cantilever deflection feedback. The principle of AFM operation is to scan the tip over the sample surface with feedback mechanisms that enable the

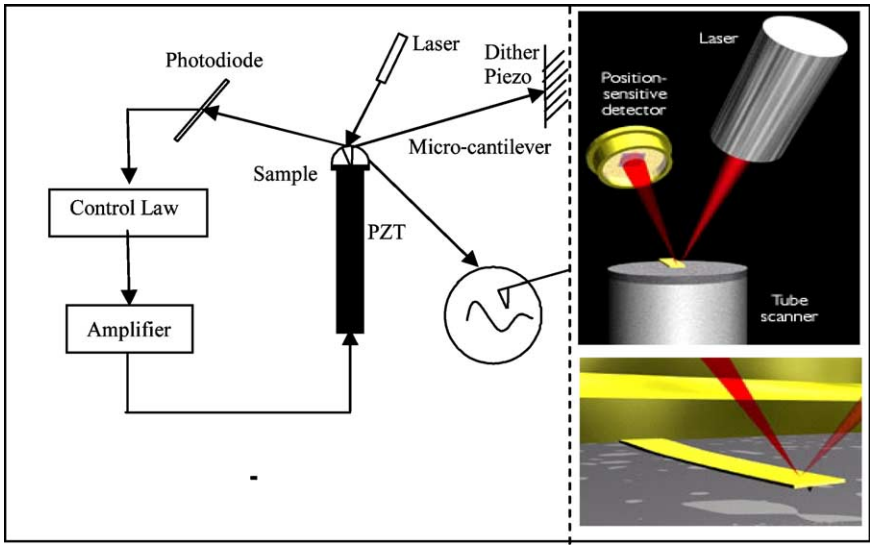

Fig. 1. Schematic of basic AFM operation (left), real micro-cantilever and components (right).

PZT scanners to maintain the tip at a constant force, or constant height above the sample surface. As the tip scans the surface of the sample, moving up and down with the contour of the surface, the laser beam deflected from the cantilever provides measurements of the difference in light intensities between the upper and lower photo detectors. Feedback from the photodiode difference signal, through software control from the computer, enables the tip to maintain either a constant force or constant height above the sample. In the constant force mode, the PZT transducer monitors real time height deviation. In the constant height mode, the deflection force on the sample is recorded.

The rest of the paper is organized as follows. In the immediately following section, the AFM operation and control modes are discussed. Three open-loop modes, namely non-contact, contact and tapping modes, are described. Section 3 provides a detailed discussion on the AFM modeling and presents both lumped-parameters and distributed-parameters modeling schemes. Some recent applications of AFM imaging systems in both molecular metrology and biological sciences are presented in Section 4, followed by the concluding remarks in Section 5.

2. AFM operational and control modes

Typically, these micro-cantilever systems are operated in three open-loop modes: (i) non-contact mode, (ii) contact mode, and (iii) tapping mode. In order to probe electric, magnetic, and/or atomic forces of a selected sample, the non-contact mode is utilized by moving the cantilever slightly away from the sample surface and oscillating the cantilever at or near its natural resonance frequency. By mounting the cantilever on a PZT element and measuring the shift from its natural resonance frequency due to sample attractive interactions, topographical information of the sample can be extracted [12]. Alternatively, the contact mode acquires sample attributes by monitoring interaction forces while the cantilever tip remains in contact with the target sample [34]. The tapping mode of operation combines qualities of both the contact and non-contact modes by gleaning sample data and oscillating the cantilever tip at or near its natural resonance frequency while allowing the cantilever tip to impact the target sample for a minimal amount of time [95,101].

Though widely practiced, open-loop operation modes of AFM exhibit the potential for chaotic behavior in the cantilever tip displacement thus rendering low resolution topographical information. As a result, recent research on AFM systems has focused on detailed numerical analysis such that this chaotic behavior region can be well defined and ideally avoided [12,101]. In addition to analytical methodology, several feedback control strategies have been developed in order to improve the AFM region operation [9,47].

The interaction forces between the tip and sample in all of the three open-loop modes can be distinctly identified on a force–displacement curve as shown in Fig. 2. When the interatomic distance is quite large, weak attractive forces are generated between the tip and the sample. As the atoms are gradually brought closer to each other, the attractive forces increase until the atoms become so close that the electron

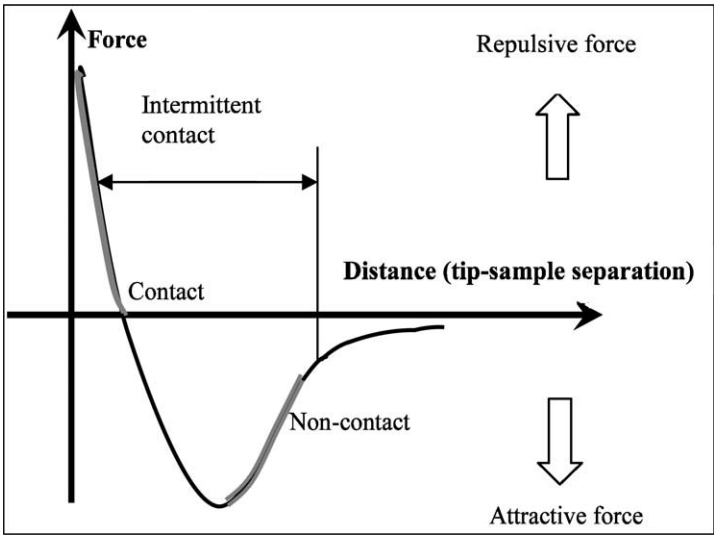

Fig. 2. Interatomic force variation versus distance between AFM tip and sample.

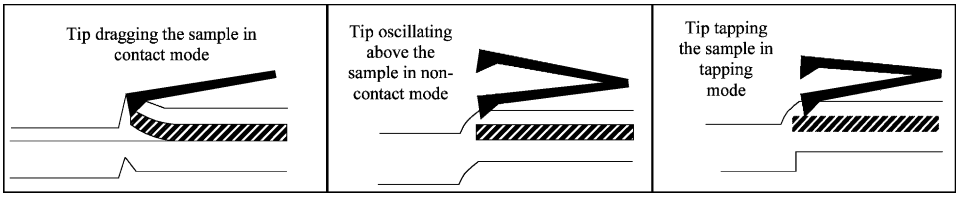

Fig. 3. Contact mode (left), non-contact mode (middle) and tapping mode (right).

clouds begin to repel each other electrostatically. This repulsive force between the atoms progressively weakens the attractive forces as the interatomic distance decreases. The interaction force becomes zero when the distance between the atoms reaches a couple of Angstroms and becomes fully repulsive when the atoms are in contact (see Fig. 2).

Fig. 3 depicts a schematic diagram of the nature of operation in all the three modes as well as the surface topography that would be generated in each mode. It can be seen that the tapping and non-contact modes reveal the surface topography of the sample to a greater extent when compared to the contact mode. Also, the operation of the AFM in contact mode damages the sample surface due to the lateral dragging forces exerted by the probe tip. The detailed description and operational characteristics of each mode is described next.

2.1. Non-contact AFM (NC-AFM) imaging systems

In this mode, the cantilever tip hovers about 50–150 Å above the sample surface to detect the attractive van der Waals forces acting between the tip and the sample,

and topographic images are constructed by scanning the tip above the surface. Since the attractive forces from the sample are substantially weaker than the forces used by contact mode, the tip must be given a small oscillation so that these small forces can be detected by measuring the change in amplitude, phase, or frequency of the oscillating cantilever. Current practice calls for detection of an amplitude shift that occurs when the tip is in the van der Waals regime. In many cases, the fluid contaminant layer is substantially thicker than the range of the van der Waals force gradient, and therefore, attempts to image the true surface with NC-AFM fail as the oscillating probe becomes trapped in the fluid layer or hovers beyond the effective range of the forces it attempts to measure. This is a major drawback of the NC-AFM imaging technique, which significantly degrades the resolution of the generated topographical images. This *barely contact mode* in practice is used to determine a set point (where tip touches sample), around which a feedback loop is utilized to control the sample positioning with respect to the tip. Another major shortfall of the NC-AFM systems is the lack of measurement of the distance between sample surface and micro-cantilever tip, i.e. z_0 in Fig. 4 (left). For highest resolution, it is necessary to measure this distance which will ultimately result in improved interaction force estimation and enhanced topographical images.

Since its invention [1,68], the NC-AFM has been increasingly used for imaging a wide class of materials, ranging from metals to semi-conductors and from polymers to biological materials [122]. The NC-AFM offers unique advantages over other contemporary scanning probe techniques such as contact AFM (C-AFM) and scanning tunneling microscopy (STM). Unlike STM and C-AFM, the absence of repulsive forces in NC-AFM permits the imaging of ''soft'' samples to provide topography with little or no contact between the tip and the sample. At the same time, the ability to resolve atomic rows, steps, or vacancies on flat (i.e. ''two-dimensional'') semi-conductor surfaces using NC-AFM has brought this microscope almost on par with the STM [36,41,115]. NC-AFM is desirable because it provides a means for measuring sample topography with little or no contact between the tip and the sample. The total force between the tip and the sample in the non-contact regime is very low, generally about 10–12 pN. This low force is advantageous for studying soft or elastic samples. A further advantage is that samples like silicon wafers are not contaminated through contact with the tip. Therefore, it does not suffer from tip or sample degradation effects that are sometimes observed after taking numerous scans with C-AFM. Since NC-AFM imaging involves the tip hovering at a fixed distance away from the sample surface, the minimal tip–sample interaction yields improved resolution over C-AFM.

2.2. Contact AFM (C-AFM) imaging systems

In this mode, also known as *Repulsive mode*, the tip is in close contact with the sample as it scans the surface (see Fig. 5). In this case, the interaction forces between the tip and the sample are mainly repulsive in nature. The examination of the van der Waals curve, as seen in Fig. 2, plotted for varying interatomic distances reveals that the slope of the curve in the contact regime is very steep. This is because, at such

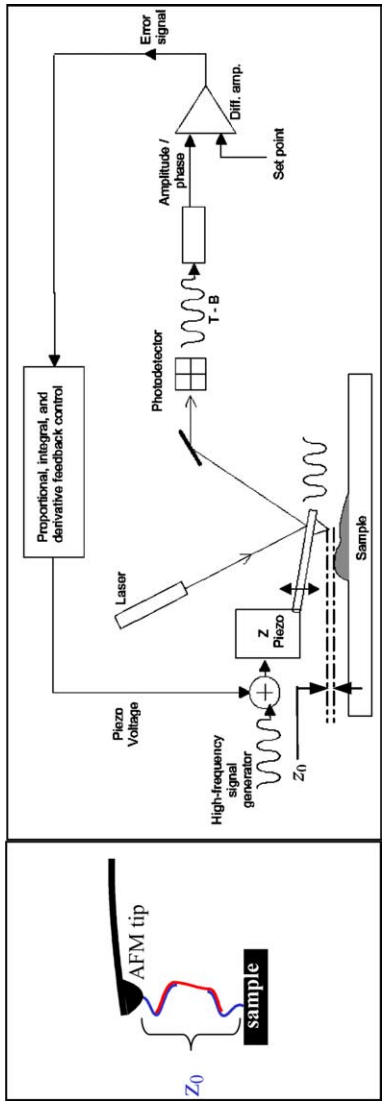

Fig. 4. Schematic diagram of non-contact AFM operation.

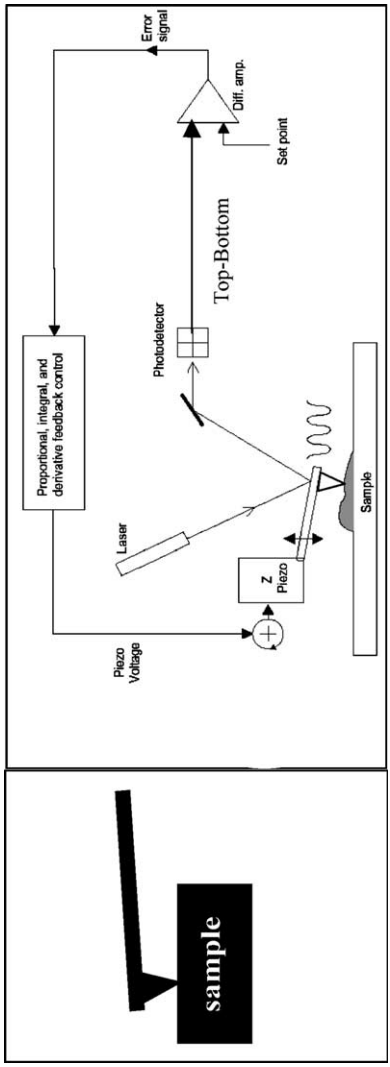

Fig. 5. Schematic diagram of contact AFM operation.

close interatomic distances, the electron clouds in the atoms repel each other electrostatically. As a result, the repulsive van der Waals force dominates any other attractive force that may tend to act.

In addition to these repulsive forces, there are two other forces generally present in C-AFM: capillary force due to the presence of a contaminant layer over the sample surface and the force exerted by the cantilever itself (this is the shear force component of the interaction force acting on the micro-cantilever). The capillary force is attractive in nature and remains constant throughout the sample (assuming that the contaminant layer is homogeneous). However, the magnitude and direction of the cantilever forces acting on the sample depend on the deflection and spring constant of the cantilever.

In C-AFM, the surface profile can be generated by operating in either of the two modes: *constant height* mode or *constant force* mode. In *constant height* mode, the PZT scanner holding the AFM tip laterally scans the surface of the sample without moving in the z-direction. The cantilever deflection thus produced as a result of the tip–sample interaction can be utilized to estimate the surface topography. The drawback of this technique is that the presence of any steep steps on the sample surface may damage the tip as it will be pushed against the surface irregularities during the scanning process.

In the *constant force* mode, which is most widely utilized, the normal force acting between the tip and the sample is kept constant through a feedback loop. A PZT positioning element is used to position the probe tip and apply the required force on the sample. Initially, the tip is brought in contact with the sample at a particular position until the required cantilever deflection is attained. Now, the tip is scanned laterally over the sample and the cantilever deflection is recorded by an optical detection system. The measured value of deflection is compared to a set value in a DC feedback amplifier and the resulting error signal from the amplifier is used to actuate the PZT positioning element by applying the required voltage. This, in turn, raises or lowers the cantilever to restore the desired deflection and thus maintains constant force (and thereby a constant height) between the tip and sample. The voltage applied by the feedback amplifier to the PZT element is a measure of the surface topography and is expressed as a function of the lateral position of the sample. This function is used to generate the surface topography of the specimen.

The main drawback of the contact mode is that the shear forces resulting from the lateral movement of the tip tend to damage soft samples and distort the features of the generated image. Therefore, this mode is not suited for examining of soft biological and polymer surfaces as it causes substantial sample degradation.

2.3. Tapping AFM (T-AFM) imaging systems

The technique of tapping mode AFM (T-AFM) is a key advance in AFM technology. This technique allows high resolution imaging of soft samples that are difficult to examine using the contact AFM technique. It overcomes problems such as friction and adhesion that are usually associated with conventional AFM imaging systems. In this mode, the cantilever is oscillated at or near its natural resonant

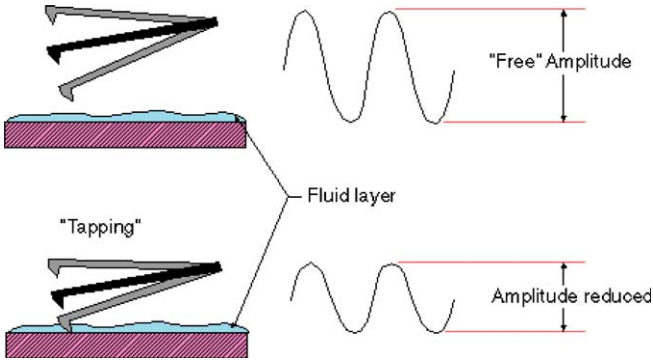

Fig. 6. Schematic of tapping mode AFM operation [87].

frequency using a PZT actuator (Fig. 6). The PZT actuator applies a force on the cantilever base and causes the cantilever tip to vibrate at amplitudes which are typically in the range of 20–100 nm when the tip is not in contact with the surface. The vibrating tip is now moved close to the sample until it begins to lightly tap the surface. During scanning, the probe tip alternately touches the surface and lifts off at frequencies of about 50–500 k cycles/s. Owing to the energy losses caused due to intermittent contacting of the tip with the surface, the amplitude of vibration changes according to the surface topography of the sample.

During tapping mode operation, the oscillation amplitude is kept constant through a feedback loop. When the tip passes over a bump in the surface, its vibration amplitude decreases due to availability of less vibrating space. On the other hand, when it passes over a depression, its vibration amplitude increases (approaching its free air amplitude). This change in oscillation amplitude is detected by the optical system and fed back to the controller which compares the measured value with the set reference value and generates an error signal. This signal actuates the PZT element that adjusts the tip–sample separation to maintain constant amplitude and thereby constant force on the sample. The error signal applied to the PZT, which is a measure of the surface irregularities in the vertical direction, is expressed as a function of the tip's lateral position and used to plot the surface topography of the sample.

3. Modeling of atomic force microscope systems

The micro-cantilever employed in an AFM is the most important and crucial component and central to its effective and efficient operation. Consequently, a thorough analysis of its dynamics and control is highly essential in order to enhance the performance of the AFM. A number of numerical models have been proposed to describe the interaction forces between the tip and the sample. Some of the representative models that depict the tip–sample interaction in tapping mode AFM have been studied, which are presented in this section.

In order to completely describe the tip–sample interaction in a tapping mode AFM, one must take into account the (i) non-linear long-range attractive forces between the tip and the sample, (ii) the non-linear mechanical compliance of the contact region, and (iii) the contact area. The contact area is a function of the surface forces that act during contact, as well as by externally applied load and by the elasticity and geometry of the materials. Some of the earlier works that have attempted to numerically simulate a tapping mode AFM [21,111] did not account for all the factors listed above. Chen et al. [21] assumed a Lennard–Jones attraction to account for the non-linear long range attractive forces between the tip and sample and a 'modified Hertz model' to account for the contact area pointed above. Alternatively, Spatz et al. [111] accounted for non-linear mechanical compliance through a simple linear contact stiffness, unaffected by surface forces. Very few works compare theoretical results with experimental findings [6]. In the model presented by Burnham et al. [18], all three factors mentioned above have been considered, with full comparison with experimental data in order to explore the limitations of the model. We present the current modeling efforts for the microcantilever dynamics in two broad classes, i.e. lumped-parameters system and distributed-parameters system.

3.1. Lumped-parameters system modeling

In the model considered by Burnham et al. [18], the cantilever is treated to be a massless spring of stiffness k having an effective mass m_e at the end and equivalent damping c. The cantilever resonates with a frequency of ω_c. Damping of the cantilever is accounted for by introducing a dashpot having an effective damping c between the base of the cantilever and the tip. As seen in Fig. 7, the position of the root of the cantilever is represented by $d(t)$ and the motion of the tip by $z(t)$.

Hence, the second order differential equation that describes the system can be given as

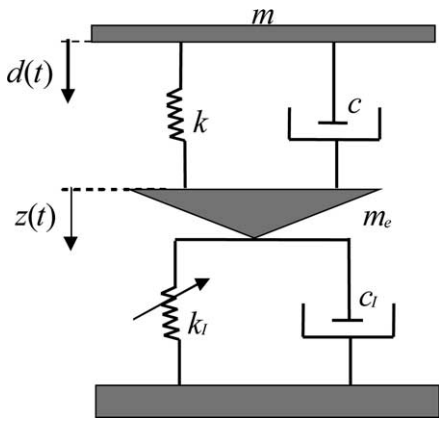

Fig. 7. Single-degree-of-freedom lumped model of a tapping mode AFM, [18].

$$m_e\ddot{z}(t) + c(\dot{z}(t) - \dot{d}(t)) + k(z(t) - d(t)) = -P(z(t)) \quad (1)$$

where $P(z(t))$ represents the force acting on the tip resulting from the tip–sample interaction, k_I is the non-linear spring stiffness and c_I is the interaction damping. The non-linear spring represents the derivative of the normalized contact load. The contact mechanics between the tip and the sample was defined by JKRS-DMT model based on Dugdale theory, [18].

3.1.1. Single mode approximation utilizing the Lennard–Jones potential

In this modeling scheme, the micro-cantilever is modeled by a single-mode approximation and the interaction between the tip and sample is described by a van der Waals (vdW) potential [9,10,49]. In addition, the forced dynamics of the system have been analyzed using the Melnikov method in order to design a controller that would eliminate the possibility of chaos in the system and thereby substantially improve the behavior of the imaging system. The cantilever is modeled as a single-degree-of-freedom (SDOF) spring–mass system. The Lennard–Jones potential has been used to account for the interaction forces between the molecules. As shown in Fig. 8, the tip is modeled as a sphere of radius R and mass m_e which is suspended by a spring of stiffness k (which corresponds to the cantilever) from a base mass m. $u(t) \in \Re$ represents the controller force input, and $F(t) \in \Re$ denotes the van der Waals attraction/repulsion force (i.e. the interaction forces).

The differential equations that describe the system can be written as follows:

$$\begin{aligned} &m\ddot{d}(t) + c(\dot{d}(t) - \dot{z}(t)) + k(d(t) - z(t)) = u \\ &m_e\ddot{z}(t) + c(\dot{z}(t) - \dot{d}(t)) + k(z(t) - d(t)) + F(t) = 0 \end{aligned} \quad (2)$$

where l_0 is the free length of the spring, c is the effective damping coefficient between the base of the cantilever and the tip, $z_0(t)$ is the distance between the equilibrium

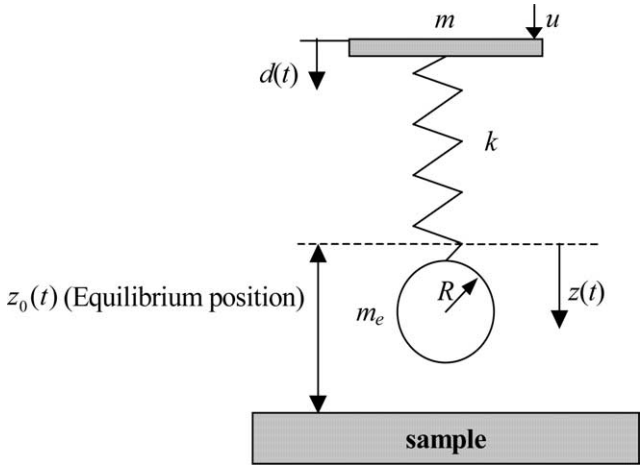

Fig. 8. Tip–sample model of Lennard–Jones potential, [10].

position of the cantilever (when only gravity is acting on it) and sample and $z(t)$ is the displacement of the cantilever tip from the equilibrium position.

The Lennard–Jones potential between two molecules is given by

$$w(r) = \frac{c_1}{r^{12}} - \frac{c_2}{r^6} = 4\beta\left[\left(\frac{\sigma}{r}\right)^{12} - \left(\frac{\sigma}{r}\right)^{6}\right] \tag{3}$$

where r is the distance between two molecules, σ is the molecular diameter, c_1 and c_2 are interaction constants, and $-\beta$ is the minimum of the potential [50,94].

Assuming that the sample and tip have molecules per unit volume of ρ_2 and ρ_1 respectively, the number of molecules in an annular region of the sample having thickness $\mathrm{d}y$ and width $\mathrm{d}x$ would be $2\pi y(\mathrm{d}y)(\mathrm{d}x)\rho_2$ (see Fig. 9). Consequently, the interaction potential between a single-molecule placed at a distance z from the sample can be evaluated using Eq. (3) as

$$\begin{aligned} w(z) &= \int_{x=z}^{\infty}\int_{y=0}^{\infty} 2\pi\rho_2 y\left(\frac{c_1}{(x^2+y^2)^6} - \frac{c_2}{(x^2+y^2)^3}\right)\mathrm{d}y\,\mathrm{d}x \\ &= 2\pi\rho_2 c_1 \int_{x=z}^{\infty}\mathrm{d}x\int_{y=0}^{\infty}\frac{y}{(x^2+y^2)^6} - 2\pi\rho_2 c_2\int_{x=z}^{\infty}\mathrm{d}x\int_{y=0}^{\infty}\frac{y}{(x^2+y^2)^3}\mathrm{d}y \\ &= \frac{2\pi\rho_2 c_1}{90z^9} - \frac{2\pi\rho_2 c_2}{12z^3} \end{aligned} \tag{4}$$

Now the interaction energy between the sphere (tip) and the surface (sample) can be computed accordingly.

That is, as seen in Fig. 10, the molecules at a distance $x + D_{ss}$ from the surface lie in a circular section of area πy^2 and thickness $\mathrm{d}x$. The number of molecules in this section can be given as $\rho_1\pi y^2\,\mathrm{d}x = \rho_1\pi(2R - x)x\,\mathrm{d}x$. Utilizing Eq. (4), the interaction energy can then be written as

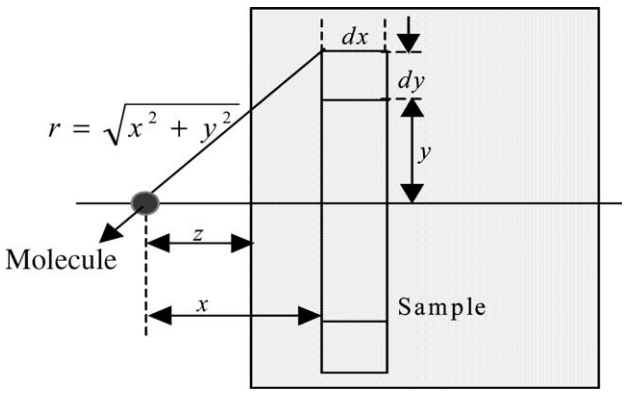

Fig. 9. Schematic of a molecule and sample surface geometry, [10].

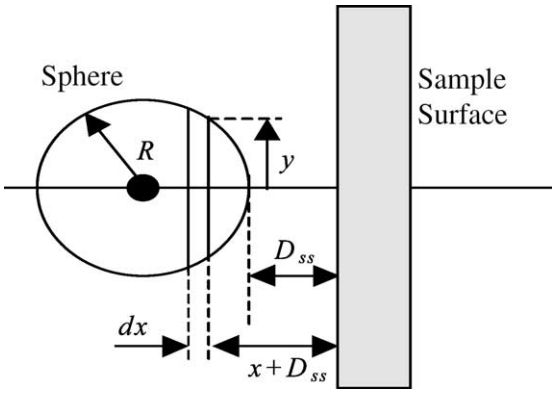

Fig. 10. Schematic of the tip (sphere) and sample (surface) interaction, [10].

$$W(D_{ss}) = \int_{x=0}^{2R} \rho_1 \pi (2R - x) x \left(\frac{2\pi\rho_2 c_1}{90(x + D_{ss})^9} - \frac{2\pi\rho_2 c_2}{12(x + D_{ss})^3} \right) dx$$
$$= \frac{A_1 R}{1260 D_{ss}^7} - \frac{A_2 R}{6 D_{ss}} \tag{5}$$

under the assumption that $R \gg D_{ss}$ (which results in $2Rx \gg x^2$). In (5), $A_1 = \pi^2 \rho_1 \rho_2 c_1$ and $A_2 = \pi^2 \rho_1 \rho_2 c_2$ are the Hamacker constants for the repulsive and attractive potentials, respectively, and D_{ss} represents the distance between the sphere and the surface as shown in Fig. 10.

The tip–sample interaction can now be modeled by the interaction potential energy given by

$$V(z, z_0) = \frac{A_1 R}{1260(z_0 - z)^7} - \frac{A_2 R}{6(z_0 - z)} \tag{6}$$

The net energy of the system scaled by the effective mass m_e can be written as

$$H(z, \dot{z}, z_0) = \frac{1}{2}\dot{z}^2 + \frac{1}{2}\omega_1^2 (z - d)^2 - \frac{D\omega_1^2}{(z_0 - z)} + \frac{\sigma^6 D \omega_1^2}{210(z_0 - z)^7} \tag{7}$$

where $\omega_1 = \sqrt{\frac{k}{m_e}}$ and $D = \frac{A_2 R}{6k}$.

By defining a set of variables $x_1 = z$ and $x_2 = \dot{z}$, then the dynamics of the tip–sample system derived from the above Hamiltonian can be recast in the following form

$$\dot{x}_1 = x_2$$
$$\dot{x}_2 = -\omega_1^2 (x_1 - d) - \frac{D\omega_1^2}{(z_0 - x_1)^2} + \frac{\sigma^6 D \omega_1^2}{30(z_0 - x_1)^8} \tag{8}$$

where $\dot{x}_1 = \frac{\partial H}{\partial x_2}$ and $\dot{x}_2 = -\left(\frac{\partial H}{\partial x_1}\right)$.

The actual system is, however, both damped and forced, and therefore not conservative. In practice, it is assumed that the damping and external forces are quite negligible and so the actual system can be considered as a perturbed Hamiltonian system. Therefore, the study of the Hamiltonian system forms the basis to analyze the behavior of the perturbed system [9,10].

3.1.2. Energy approach

A different but complementary approach, known as *Energy approach* has been used to analyze the tip–sample interaction [5]. The advantage of using this method is that it does not necessitate the solution procedure of differential equations that describe the dynamic motion of the oscillating cantilever. Therefore, the need to find a realistic model describing the tip–sample interaction in terms of the non-linear force–distance dependencies and damping effects is omitted. This method is applicable to a variety of scanning probe microscopes operating in different dynamic modes and proves to be very important, especially when used to interpret phase data obtained in tapping mode. The basic principle utilized in this method is that, for any dynamic system in equilibrium, the average energy input must equal the average energy output or dissipated.

For an AFM operating in dynamic mode, the power input given is the cantilever oscillation fed from an external driver represented by $\overline{P_{\text{in}}}$. The average power dissipated by the motion of the cantilever is represented by $\overline{P_{\text{o}}}$ and by tip–sample interaction is given by $\overline{P_{\text{tip}}}$. Therefore, one can write

$$\overline{P_{\text{in}}} = \overline{P_{\text{o}}} + \overline{P_{\text{tip}}} \tag{9}$$

The term $\overline{P_{\text{tip}}}$ characterizes the tip–sample interaction and can be computed from Eq. (9).

A simplified model is used in this case to describe the dynamic system that comprises of a spring and two dampers, as shown in Fig. 11.

The spring, characterized by constant k, describes the mode through which power is transmitted from the external driver $d(t)$ to the oscillating tip $z(t)$, c_1 represents the damping coefficient corresponding to the relative motion between the cantilever tip and base and c_2 represents the damping coefficient due to the movement of the

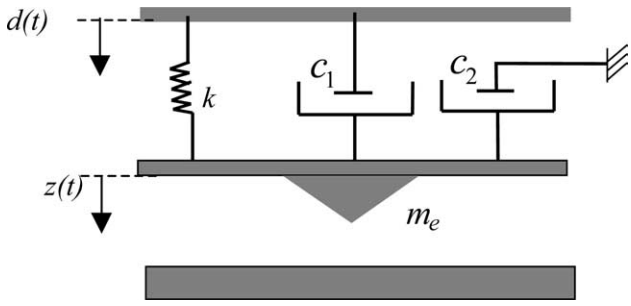

Fig. 11. Model describing the dynamic AFM system, [5].

cantilever in some surrounding medium. Therefore, the instantaneous power fed to the system can be given as

$$P_{\text{in}}(t) = F_{\text{d}}(t)\dot{d}(t) = k[z(t) - d(t)]\dot{d}(t) \tag{10}$$

Assuming that the cantilever is driven sinusoidally with amplitude A_{d} and frequency ω, we have $d(t) = A_{\text{d}}\cos(\omega t)$ and $z(t) = A\cos(\omega t - \varphi)$ where A and φ are the oscillation amplitude and the frequency shift at the tip, respectively. The average power for a particular oscillation cycle can be obtained by integrating over a time period $T = \frac{2\pi}{\omega}$ as

$$\overline{P_{\text{in}}} = \frac{1}{T}\int_0^T P_{\text{in}}(t)\,\mathrm{d}t = \frac{1}{2}k\omega A_{\text{d}}A\sin\varphi \tag{11}$$

The factor $\overline{P_{\text{o}}}$ is constituted by the damping that occurs due to the relative motion of the tip relative to the base, which corresponds to

$$P_{01}(t) = |c_1[\dot{z}(t) - \dot{d}(t)]\dot{z}(t)| \tag{12}$$

Similarly, the damping that occurs due to motion of the tip in the surrounding medium, such as air, corresponds to

$$P_{02}(t) = c_2\dot{z}^2(t) \tag{13}$$

The average power distribution given over the cycle can then be computed as follows

$$\begin{aligned}\overline{P_{01}} &= \frac{1}{T}\int_0^T P_{01}(t)\,\mathrm{d}t \\ &= \frac{1}{\pi}c_1\omega^2 A\left[(A - A_{\text{d}}\cos\varphi)\arcsin\left(\frac{A - A_{\text{d}}\cos\varphi}{\sqrt{A^2 + A_{\text{d}}^2 - 2AA_{\text{d}}\cos\varphi}}\right) + A_{\text{d}}\sin\varphi\right]\end{aligned} \tag{14}$$

and

$$\overline{P_{02}} = \frac{1}{T}\int_0^T P_{02}(t)\,\mathrm{d}t = \frac{1}{2}c_2\omega^2A^2 \tag{15}$$

Since it is assumed that $A \gg A_{\text{d}}$ when the cantilever is driven at or near its resonance frequency, it yields

$$\overline{P_{\text{o}}} = \frac{1}{2}c\omega^2A^2 \quad \text{with } c = c_1 + c_2 \tag{16}$$

where c is the effective damping coefficient. The equivalent system can now be redrawn as shown in Fig. 12.

Consequently, the term $\overline{P_{\text{tip}}}$ can be easily computed by finding the difference between the input power and the power dissipated due to damping. Furthermore, by expressing the damping constant c in terms of experimentally accessible quantities such as the spring constant k, the quality factor Q_{cant} and the natural resonant frequency ω_0 of the free oscillating cantilever $c = \frac{k}{Q_{\text{cant}}\omega_0}$, it yields

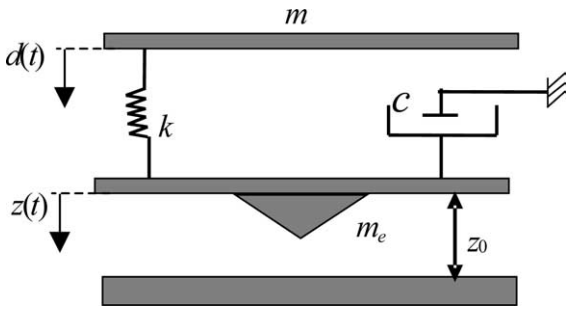

Fig. 12. Equivalent model of the AFM model in Fig. 11, [5].

$$\overline{P_{\text{tip}}} = \overline{P_{\text{in}}} - \overline{P_0} = \frac{1}{2}\frac{k\omega}{Q_{\text{cant}}}\left[Q_{\text{cant}}A_{\text{d}}A\sin\varphi - A^2\frac{\omega}{\omega_0}\right] \tag{17}$$

Thus, the tip–sample interaction characterized by the term $\overline{P_{\text{tip}}}$ can be studied easily.

Applying Eq. (17) for an AFM operating in tapping mode and by considering the free oscillation amplitude $A_{\text{o}} = Q_{\text{cant}}A_{\text{d}}$, it yields

$$\overline{P_{\text{tip}}} = \frac{1}{2}\frac{k\omega_0}{Q_{\text{cant}}}[A_0A_{\sin\varphi} - A^2] \tag{18}$$

It can be seen that if the oscillation amplitude A is kept constant through a feedback loop, which is commonly done in tapping mode, simultaneously acquired phase data can be interpreted in terms of energy dissipation. When analyzing such phase images [22,64,86], one has also to consider the fact that the phase may also change due to the transition from net attractive to net repulsive interaction between the tip and the sample [4,7].

3.1.3. High-Q dynamic force microscopy

In [52], a new dynamic force microscopy technique has been presented which allows the use of tapping mode AFM for imaging of soft materials in liquids by operating in the picoNewton regime. The low quality factor (Q) of the cantilever was increased up to three orders of magnitude by the implementation of a positive feedback control. The technique also includes a phase-locked loop unit to track the resonance of the cantilever. Experiments and computer simulations indicate that the tip–sample forces are below 100 pN, about two orders of magnitude lower than in conventional tapping mode atomic force microscopy. Furthermore, the spectroscopic ability is greatly enhanced. This technique has demonstrated tremendous potential for imaging living cells.

This system can be approximated as two springs in series; one is the cantilever with a spring constant k_{c}, and the other represents the tip–sample force with a spring constant k_{ts}, equal to the force gradient. Thus, the effective spring constant of the cantilever changes according to $k'_{\text{c}} = k_{\text{c}} - k_{\text{ts}}$, and the resonance shifts from f_0 to $f'_0 = f_0(1 - \frac{k_{\text{ts}}}{k_{\text{c}}})^{\frac{1}{2}}$.

In conventional dynamic force microscopy, the cantilever response (z) to the incident forces (F) can be expressed as $z(\omega) = X(\omega)F(\omega)$, in which the cantilever transfer function (X) can be approximated as that of a damped harmonic oscillator:

$$X(\omega) = \frac{\omega_0^2 k}{\omega_0^2 - \omega^2 + \mathrm{i}\omega_0\omega/Q} \tag{19}$$

where ω_0 and ω are the resonant and incident force frequencies respectively, k is the spring constant of the cantilever, and Q is the quality factor. The forces acting on the cantilever are the driving forces that excite the cantilever through $F_{\text{int}} = F_0 \mathrm{e}^{\mathrm{i}\omega t}$, the thermal force and the interaction force between the tip and the sample (F_{int}). During the cantilever oscillation, the interaction force depends on time as the tip–sample distance is $z \cong z_0 + A\mathrm{e}^{\mathrm{i}\omega t}$, that is,

$$\begin{aligned} F_{\text{int}}(z) &= F_{\text{int}}(z_0) + \frac{\mathrm{d}F_{\text{int}}}{\mathrm{d}z}(z_0)\Delta z + \frac{1}{2}\frac{\mathrm{d}^2 F_{\text{int}}}{\mathrm{d}z^2}(z_0)\Delta z^2 + \cdots \\ &= F_{\text{int}0} + F_{\text{int}1}\mathrm{e}^{\mathrm{i}\omega t} + F_{\text{int}2}\mathrm{e}^{\mathrm{i}2\omega t} + \cdots = F_{\text{int}}(t) \end{aligned} \tag{20}$$

Neglecting the thermal force, the total force acting on the cantilever is

$$\begin{aligned} F_{\text{tot}} &= F_{\text{int}0} + (F_0 + F_{\text{int}1})\mathrm{e}^{\mathrm{i}\omega t} + F_{\text{int}2}\mathrm{e}^{\mathrm{i}2\omega t} + \cdots \\ &= F_{\text{int}0} + F_1(\omega) + F_2(2\omega) + \cdots \end{aligned} \tag{21}$$

which produces a cantilever response $z = X(\omega)F_{\text{tot}}$ as

$$z = z_0 + A_1\mathrm{e}^{\mathrm{i}(\omega t - \varphi_1)} + A_2\mathrm{e}^{\mathrm{i}(2\omega t - \varphi_2)} + \cdots = z_0 + z_1(\omega) + z_2(2\omega) + \cdots \tag{22}$$

The cantilever motion is sinusoidal in air and vacuum, but it is anharmonic in liquid with a significant contribution of higher harmonics. When the driving frequency is close to resonance ($\omega = \omega_0$), the contribution of the higher harmonics of the interaction force, $F_n(n\omega_0)$ (where $n > 1$), to the cantilever motion, $z_n(n\omega_0)$ is more significant as the resonance peak is broader, i.e. lower Q.

The low quality factor Q of the cantilever in liquid can be increased to Q_{eff} by introducing a controller that feeds back the cantilever motion with a defined transfer function $C(\omega)$ to the driving force unit, as shown in Fig. 13 (left). Thus, the modified cantilever response function can be given as

$$X'(\omega) = \frac{X(\omega)}{1 \pm C(\omega)X(\omega)} \tag{23}$$

The frequency-dependent transfer function $C(\omega)$ is given as

$$C(\omega) = \mathrm{i}\frac{\omega}{\omega_0}k\left(\frac{1}{Q} - \frac{1}{Q_{\text{eff}}}\right) \tag{24}$$

Assuming that the driving frequency is very close to the resonant frequency of the cantilever (valid for high effective quality factors used in this technique), we get

$$C(\omega) = \mathrm{i}k\left(\frac{1}{Q} - \frac{1}{Q_{\text{eff}}}\right) = \mathrm{e}^{\mathrm{i}\pi/2}G \tag{25}$$

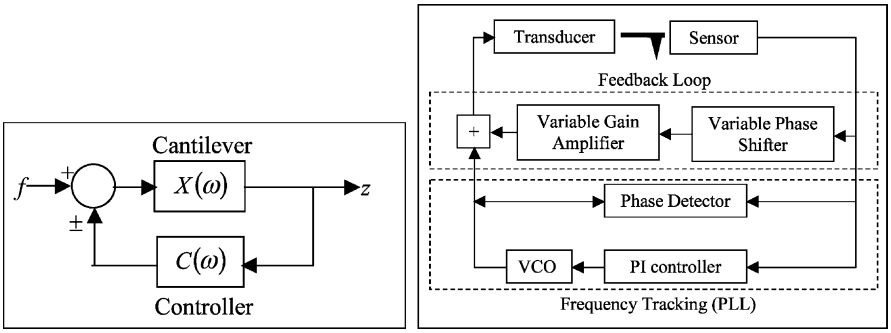

Fig. 13. Block diagram of the cantilever motion control (left), schematic of the experimental setup (right), [52].

Fig. 13 (right) shows a schematic of the experimental setup. The positive feedback loop monitors the response of the cantilever detected by the sensor element, composed of the photodiode detector and a lock-in amplifier, giving a signal proportional to the main harmonic of the cantilever oscillation $z_1 = A_1 e^{i(\omega t-\varphi)}$. This signal is shifted 90° by the variable phase shifter, amplified with a gain G by the variable gain amplifier, and the processed signal is finally added to the driving signal of the cantilever. In other words, the cantilever is excited by two forces, the standard driving force $F_{ext1} = F_0 e^{i\omega t}$ and a cantilever motion-dependent force $F_{ext2} = G e^{i\pi/2} A_1 e^{i(\omega t-\varphi)}$. Thus, the motion of the cantilever can be described by the differential equation of a damped harmonic oscillator driven by F_{ext1} and F_{ext2},

$$m\frac{d^2z}{dt^2} + \gamma\frac{dz}{dt} + kz = F_0 e^{i\omega t} + G e^{i\pi/2} A_1 e^{i(\omega t-\varphi)} + F_{int}(z) \tag{26}$$

where m is the effective mass of the cantilever and γ is the damping constant of the system due to the hydrodynamic damping between the cantilever and the environment and the internal friction of the cantilever. As long as the cantilever oscillation is sinusoidal, the velocity of the cantilever can be expressed as

$$\frac{dz}{dt} = \omega e^{i\pi/2} z \tag{27}$$

Eq. (26) can be written as

$$m\frac{d^2z}{dt^2} + \gamma\frac{dz}{dt} + kz = F_0 e^{i\omega t} + \frac{G}{\omega}\frac{dz}{dt} \tag{28}$$

$$m\frac{d^2z}{dt^2} + \gamma_{eff}\frac{dz}{dt} + kz = F_0 e^{i\omega t} \tag{29}$$

where the effective damping constant is $\gamma_{eff} = \gamma - \frac{G}{\omega}$. As a result, the changed Quality factor is given as $Q_{eff} = \frac{m\omega_0}{\gamma_{eff}}$.

The experimental set-up shown in Fig. 13 (right) also includes a phaselocked loop (PLL) to track the resonant frequency of the system. Although this might be

optional, it improves the performance of the microscope. The PLL produces a driving signal of the form $F_{ext} = F_0 e^{i\omega t}$ and monitors the cantilever response, adjusting the driving frequency, $\omega = 2\pi f$, to maintain a phase difference of 90° compared to the driving signal, i.e. maintaining the system at resonance.

3.1.4. Modeling tapping mode AFM using electric circuit simulator

In [93], the AFM tip is considered as a forced oscillator and the sample represented by an elastic material having adhesive properties. An equivalent electrical circuit, analogous to the tip–sample model is also proposed which offers a way to simulate the system using an electrical circuit simulator.

The sample is modeled as an equivalent spring constant (contact stiffness) and a damping effect, which arises due to the internal viscosity of the sample. The equivalent mass of the sample is considered negligible in this work. Interaction forces due to adhesion, surface charges, and some other sources are defined as a single-valued function of the distance between the tip and sample surface ($x_t - x_s$). In order to estimate the spring constant k_s of the sample, the Hertz model applied to deformable bodies can be utilized. When the model is applied to the tip–sample interaction, the equivalent spring constant is given by:

$$k_s = \frac{3}{2} E^* \sqrt{R z_{def}} \tag{30}$$

where R is the effective radius of the tip, E^* is the effective elastic modulus of the system, and z_{def} is the deformation of the sample. This value changes with force applied to the sample. Therefore, a nominal value of force is needed to estimate the spring constant of the sample. The best choice of this value is the adhesion force (F_{adh}), since it is observed when there is no external force applied to the tip. Also, the forces observed in tapping modes are approximately equal to this value. The equivalent spring constant can be written in terms of this force as

$$k_s = \sqrt[3]{6E^{*2} R F_{adh}} \tag{31}$$

The most important approximation here is to assume that this spring constant would be applicable also when the surface is pulled up. That is mainly because the forces of adhesion are effective at very short distances and, therefore, the surface is pulled up from a small volume in the vicinity of the tip. This is similar to the repulsion where the force is applied from a small contact area but to the opposite direction. With this assumption, the resulting coupled differential equations of motion become

$$m \frac{d^2 x_t}{dt^2} + \frac{m\omega_0}{Q} \frac{dx_t}{dt} + k_t(x_t - \alpha_{sp}) - F(x_t - x_s) = A\cos(\omega t) \tag{32}$$

$$\gamma_s \frac{dx_t}{dt} + k_s x_s - F(x_t - x_s) = 0 \tag{33}$$

where m, k_t, ω_0, ω, Q, α_{sp}, and A are the mass, spring constant, free resonance frequency, excitation frequency, quality factor, set point, and driving amplitude of the tip, respectively, and γ_s and k_s are the internal damping coefficient and contact

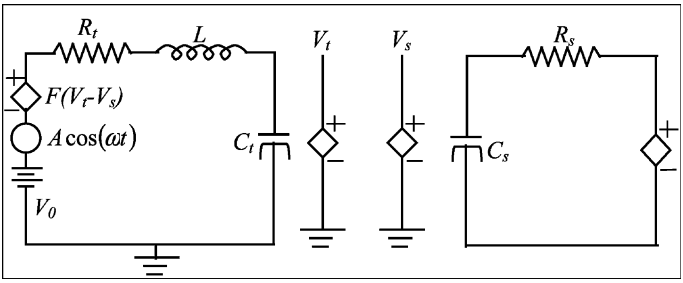

Fig. 14. Equivalent electrical circuit of the mechanical model; the cantilever-tip system (left) and the sample (right), [93].

stiffness of the sample. x_t and x_s represent the positions of the tip and sample surface, respectively, as measured from the equilibrium point of the sample.

The equivalent electrical circuit representing the tip–sample model is obtained by replacing the masses with inductors, springs with capacitors, damping with resistors, and forces with voltages. The interaction force is represented by a non-linear controlled source. Fig. 14 shows the resulting electrical circuit. Diamond shaped symbols represent controlled voltage sources. $F(V_t - V_s)$ represents the force of interaction between tip and sample. Constant voltage source, V_0 is used to adjust the set point.

The coupled differential equations for the charges q_t and q_s of the capacitors can be written as

$$L\frac{d^2q_t}{dt^2} + R_t\frac{dq_t}{dt} + \frac{q_t}{C_t} - F(q_t - q_s) = A\cos(\omega t_0) + V_0 \tag{34}$$

$$R_s\frac{dq_s}{dt} + \frac{q_s}{C_s} - F(q_t - q_s) = 0 \tag{35}$$

The complete analogy between the mechanical and electrical system makes it possible to simulate the mechanical problem with an electrical circuit simulator such as SPICE, [76].

3.2. Distributed-parameters system modeling

Extensive research has been done on modeling and characterization of AFM tip–sample surface interaction. As demonstrated in the preceding section, current modeling practices call for simple lumped models where a set of ordinary differential equations (ODE) govern the system dynamics. For example, Hsu and Fu [47] utilized an ODE based interaction model and feedback linearization and singular perturbation techniques to design an output, high-gain feedback sample surface tracking controller. Ashhab et al. [9] also utilized the Melnikov method to analyze the system dynamics and subsequently developed a proportional/derivative based feedback strategy to inject artificial damping such that the possibility of chaotic operation is removed. However, the distributed nature of structural flexibility in the micro-

cantilever is becoming an issue of increasing concern due to its direct influence on the image resolution. In contrast to the previously utilized lumped modeling methods, we present here a general distributed-based modeling approach that reveals greater insight into the fundamental characteristics of the dynamics [31,32]. In order not to disturb the focus of the paper, which is on the review of AFM rather than technical modeling, we refer interested readers to our recent line of publications in distributed-parameters system modeling, [25,53,54,58]. Here, we present an overview of this approach where the cantilever–sample interaction system model of [9] is extended to include the distributed nature of the micro-cantilever assembly. Specifically, the system model of the cantilever–sample interaction system of Fig. 15 encompasses the flexibility effects and distributed mass characteristics along the beam through the following dynamics.

By utilizing the extended Hamilton approach, the kinetic and potential energies of the system can be written in the form:

$$\text{kinetic energy} = T = \frac{1}{2}\rho \int_0^L \{z_t(x,t) + \dot{d}(t)\}^2 \mathrm{d}x + \frac{1}{2} m \dot{d}^2(t) + \frac{1}{2} m_e (z_t(L,t) + \dot{d}(t))^2 \tag{36}$$

$$\text{potential energy} = V = \frac{1}{2} EI \int_0^L z_{xx}^2(x,t)\mathrm{d}x \tag{37}$$

where ρ is the micro-cantilever linear density, $z(x,t)$ is the lateral displacement of the micro-cantilever, $d(t)$ represents the base motion (i.e. PZT positioner displacement), m is the total mass of the base, m_e is the tip mass and EI is the micro-cantilever rigidity. Considering the damping and interaction forces as non-conservative forces in the extended Hamilton approach, we have

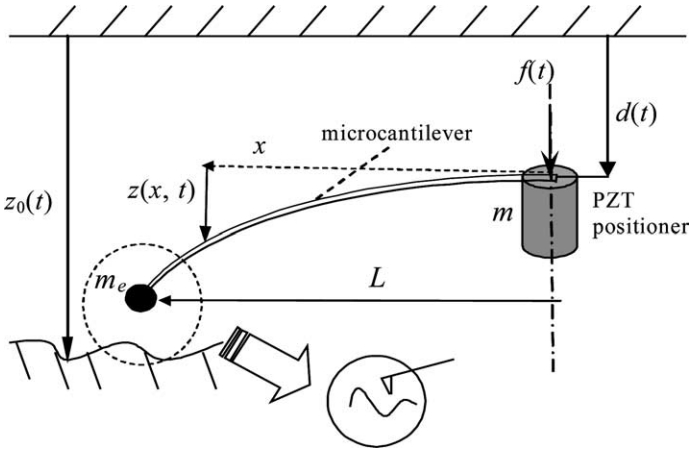

Fig. 15. Schematic of AFM system modeling in distributed-parameter configuration.

$$\delta W_{\mathrm{nc}} = -Bz_{\mathrm{t}}(x,t)\delta z - Cz_{xt}(x,t)\delta z + f\delta d(t) + f_{\mathrm{I}}\delta z(L,t) \tag{38}$$

where $\delta()$ represents the variational operator, f is the control force at the base, f_{I} is the atomic interaction force, and B and C are the damping coefficients associated with the cantilever structural properties [11,32].

The equations of motion can now be obtained using the Hamilton's principle

$$\int_{t_1}^{t_2} (\delta T - \delta U + \delta W)\mathrm{d}t = 0 \tag{39}$$

Consequently, the beam equation can be obtained as [25,53]

$$\begin{aligned} &(\rho L + m + m_{\mathrm{e}})\ddot{d}(t) + m_{\mathrm{e}} z_{tt}(L,t) + \int_0^L \rho z_{tt}(x,t)\mathrm{d}x = f(t) + f_{\mathrm{I}}(t) \\ &\rho(z_{tt}(x,t) + \ddot{d}(t)) + Bz_{\mathrm{t}}(x,t) + Cz_{xt}(x,t) + EIz_{xxxx}(x,t) = 0 \end{aligned} \tag{40}$$

where $u(x,t) \in \Re$ represents the lateral displacement of the micro-cantilever beam (*note*: the subscript $()_{\mathrm{t}}$ and $()_x$ indicate the partial derivative with respect to the time variable t and position variable x, respectively), $d(t)$, $\dot{d}(t)$, $\ddot{d}(t)$ represent the base unit displacement (i.e., a PZT positioner), velocity, and acceleration signals, respectively.

The atomic interaction force $f_{\mathrm{I}}(t)$ can be described by the following relationship [12]

$$f_{\mathrm{I}} = \frac{H_1}{[z_0(t) - z(L,t) - d(t)]^2} - \frac{H_2}{30[z_0(t) - z(L,t) - d(t)]^8} \tag{41}$$

with H_1 and H_2 representing the Hamacker constants, and $z_0(t)$ representing the distance from the fixed base frame coordinate to the sample surface when $z(L,t) = d(t) = 0$. The boundary conditions for the distributed system of (40) are given by the following

$$z(0,t) = z_x(0,t) = z_{xx}(L,t) = 0, m_{\mathrm{e}}(\ddot{d}(t) + z_{tt}(L,t)) - EIz_{xxx}(L,t) = f_{\mathrm{I}}(t) \tag{42}$$

The cantilever tip displacement $z(L,t)$ of (42) is measured from the base position. Furthermore, the total cantilever tip displacement is assumed to be constrained by the following inequality

$$(z_0(t) + z(L,t) + d(t)) \geqslant R \tag{43}$$

where R denotes some positive constant; hence, the interaction force $f_{\mathrm{I}}(t)$ can be upper bounded (i.e. $f_{\mathrm{I}}(t) \in L_\infty$) [31,32] by

$$|f_{\mathrm{I}}| \leqslant \frac{H_1}{R^2} + \frac{H_2}{30R^8} \tag{44}$$

4. Application of AFM imaging systems

Due to its inherent advantages, AFM's find a variety of applications that range from nanofabrication (e.g. semi-conductors) to biological materials (e.g. studying DNA structure) [55,70,81,82,97,98,106,109]. Non-contact imaging at low tip oscil-

lation amplitudes provides extremely high resolution imaging without the tip damage which occurs when using tapping mode techniques. The diverse applications of AFM can be broadly classified into two major categories: *Molecular Metrology* and *Biological Sciences*. The former category mainly deals with engineering applications that span over various manufacturing fields such as testing of electronics components and fabrication of miniature mechanical parts. On the other hand, the latter category deals with the implementation of AFM in crucial biological applications to determine cell/cell or cell/protein interactions and to observe cell movements in living species. These applications are discussed next.

4.1. Molecular metrology

This section gives an overview of some of the vital applications of AFM in mechanical manufacturing.

4.1.1. Studies of metallic surfaces and micro-structures

Reliable measurements of micro-structural parameters on the nanometer scale are of great relevance for developing new alloys and for quality control in manufacturing processes. AFM is a proven imaging and measurement tool which complements other microscopic techniques for such application. AFM also provides additional capabilities and advantages relative to other microscopies, including superior resolution, 3D measurements, little or no sample/substrate preparation, and operation in ambient air or fluid. Metallic micro-structures cover a range of many orders of magnitude in size. Therefore, different microscopic techniques like optical microscopy, scanning electron microscopy (SEM) and, for even higher resolution, transmission electron microscopy (TEM), are in use for visualization of these micro-structures. AFM is a very useful supplement to these techniques with scan sizes ranging from 100 μm down to several nanometers, comparable to and, in some cases, exceeding the very high magnifications achievable with TEM. This large dynamic range is illustrated in the images shown in Fig. 16, where the micro-structures of a perlitic steel, martensite, and an X' precipitated nickelbase superalloy are resolved clearly with the AFM [57,121,123].

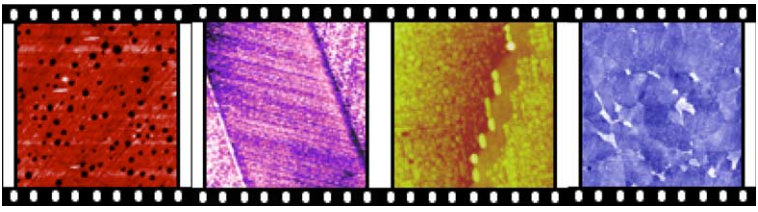

Fig. 16. Micro-structure of perlitic, martensite and an X' precipitated nickelbase superalloy, [121].

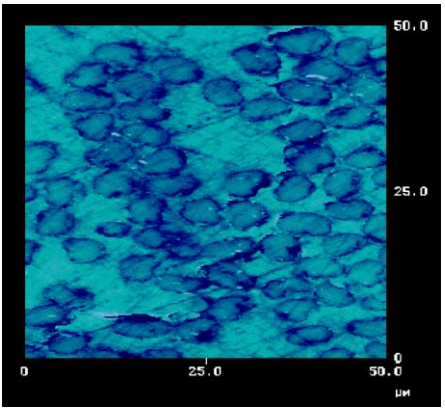

Fig. 17. Imaging of the hardness of the carbon fibers embedded in softer epoxy [37,75].

4.1.2. Nanomechanical studies

With the advent of AFM, material properties such as "hardness" cannot only be tested for, but can also be visualized. Using a scanning probe microscope, it is now possible to see the different hardnesses of a composite material and visually distinguish between the hard and soft regions (see Fig. 17). That is, the AFM enables one to obtain images, in which resolution is based solely on the differences between the hard and soft regions of the material image [17,37,75].

4.1.3. Nanoindentation, in-situ loading and investigation of cracks

AFM's can also be used to plastically indent the specimen surface. This in situ imaging ability eliminates the need to move the sample, switch tips, relocate the area for scanning, or use an entirely different instrument to image the indentation. The nanoindentation capability also includes the ability to perform scratch and wear tests using the same cantilevers. A major application of nanoindentation is the measurement of mechanical properties of thin films, such as diamond-like carbon, using indentation to investigate hardness, and scratch or wear testing to investigate film adhesion and durability. Recent studies have been done on chemical/mechanical polishing samples (CMP), used in the semi-conductor industry, polymers, such as polyimide films, and biological samples such as bovine and human sperm nuclei. Indentation techniques (e.g. Vickers hardness testing) are well-known methods in the field of materials science for fast estimations of yield stress and tensile strength with hardness values calculated from optical inspection of the indentation size. With AFM, indentation techniques can now be performed at much smaller sizes and force scales. For "nanoindentation", diamond tips (see Fig. 18) are used instead of the standard Si_3N_4 tips [77–79,83]. Using a diamond tip mounted to a metal-foil cantilever, a surface can be indented and the indentation can be imaged. Indentation sizes can be reduced to 10 nm or less, which makes it possible for local studies of the mechanical properties of the micro-structure [71]. Properties such as film adhesion and durability can also be studied using indentation cantilevers. The

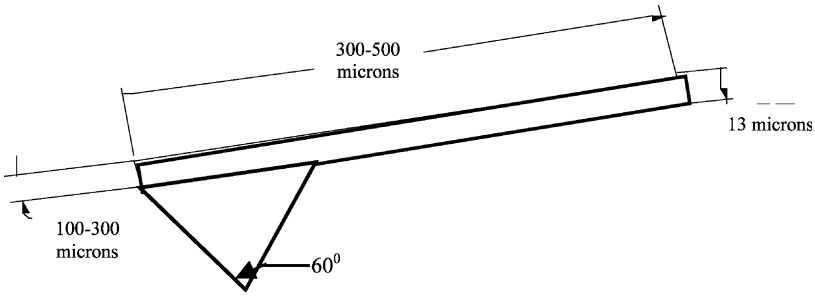

Fig. 18. Diamond tip held to metal-foil cantilever in nanoindentation [78,79].

nanoindentation capability includes the ability to perform scratches at various forces, rates, lengths and angles [35,56,102,118].

Another application of AFM is imaging of defects like cracks, dislocations and pores. The high resolution capability of AFM permits study of the processes of brittle and ductile crack growth in detail. Fig. 19 shows two images from a loaded mode I crack in a single-crystalline specimen of NiAl. The crack grows after loading (from the left to the right image) in a quasi-stable brittle manner in steps of nearly 1 μm length. In both images, the high-stressed red region around the crack tip was caused by small elastic displacements. The high stress intensity of the crack produces a small elastic depression zone with a depth of only some 10 nm. These elastic displacements around the brittle crack tip are only visible with the high vertical resolution of the AFM [38,39,51].

4.1.4. Determination of elasticity

Force modulation microscopy (FMM), an extension of AFM imaging, has been used extensively for the characterization of a sample's mechanical properties and in applications such as imaging composition changes in a composite material, analyzing polymer homogeneity, and detecting contaminants in manufacturing processes. In FMM mode, the AFM tip is scanned in contact with the sample, and the z feedback loop (vertical displacement of the micro-cantilever base) maintains a constant cantilever deflection (as for constant-force mode AFM). In addition, a periodic signal is applied to either the tip or the sample. The amplitude of cantilever modulation that

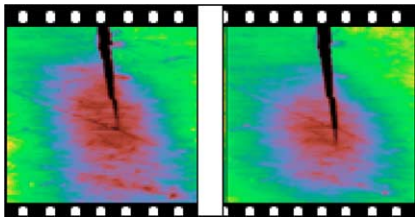

Fig. 19. Crack images of a single-crystalline specimen of NiAl obtained by AFM [38,39].

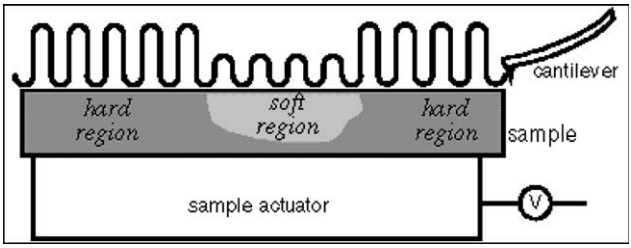

Fig. 20. Variation of the cantilever oscillation amplitude as function of the mechanical properties of the sample [3,27].

results from this applied signal varies according to the elastic properties of the sample, as shown in Fig. 20.

The system generates a force modulation image, which is a map of the sample's elastic properties, from the changes in the amplitude of cantilever modulation. The frequency of the applied signal is on the order of hundreds of kilohertz, which is faster than the z feedback loop is set up to track. Thus, topographic information can be separated from local variations in the sample's elastic properties, and the two types of images can be collected simultaneously [3,27,99].

4.1.5. Identifying various surface compositions

Lateral force microscopy (LFM) is an extension to the Scanning probe microscopy (SPM) technique in which the relative differences in the surface frictional characteristics are used to identify varying surface compositions. In this technique, the probe is scanned sideways on a fast axis and also forward-back on a slow axis, as shown in Fig. 21. The resulting twisting or torsion of the cantilever depends on the frictional characteristics of the surface and varies as it moves from one surface to another. A laser detector with four quadrants is used to simultaneously measure and record the topographic and lateral force data. As depicted in Fig. 22, the LFM image of a magnetic recording head identifies individual grains not seen in the topographical image [46].

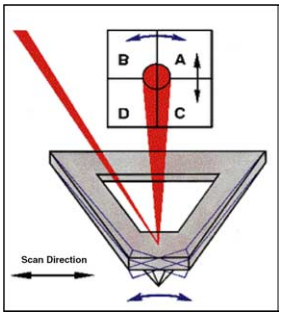

Fig. 21. Operation of lateral force microscopy (LFM), [46].

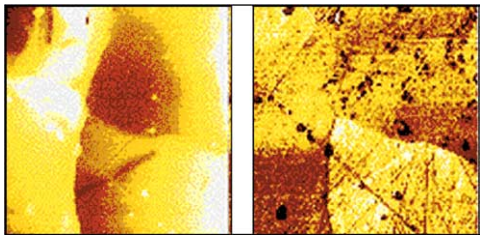

Fig. 22. LFM image (right) and topography (left) of magnetic recording head, [46].

4.1.6. Electrical properties characterization

Electric force microscopy (EFM) and surface potential (SP) imaging are two AFM techniques which characterize materials for electrical properties. A conductive AFM tip interacts with the sample through long-range Coulomb forces. These interactions change the oscillation amplitude and phase of the AFM cantilever, which are detected to create EFM or SP images. In an EFM, the images of the phase, frequency, or amplitude of the cantilever oscillation is plotted. This phase, frequency, or amplitude is related to the gradient of the electric field between the tip and the sample. In a SP image, variations in the surface potential on the sample are plotted. A voltage carrying AFM tip also enables electrical modification of materials on or beneath the surface. In such generated images (see Fig. 23), the shallow pit near the center, not distinguishable from many similarly-sized features in view, was identified in an SP image. The pit was about 160mV higher in potential than the surrounding area [103].

Other applications of these techniques include electrical failure analysis, detecting trapped charges, quantifying contact potential difference (CPD) between metals and/or semi-conductors, mapping relative strength and direction of electric polarization, testing electrical continuity, and performing electrical read/write.

4.1.7. Molecular electronics

Saifullah et al. have used an AFM with a carbon nanotube tip to image co-planar metal–insulator–metal junctions and measure nanometer scale gaps between the metallic junctions with a high degree of accuracy. Fig. 24 shows the AFM image of coplanar electrodes with narrow gaps in between them. The sizes of the gaps were

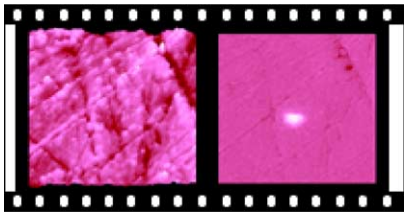

Fig. 23. Topography (left) and SP images of Aluminum (right), [103].

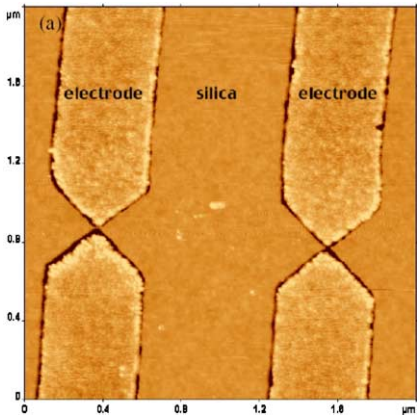

Fig. 24. AFM image of coplanar electrodes with narrow gaps.

less than or equal to 5 nm and the smallest gap measured using the AFM was approximately 2 nm.

4.1.8. Nanofabrication

A scanning probe microscope (SPM) and an atomic force microscopy (AFM) have become powerful tools for fabrication of semi-conductor nanoscale structures. An SPM oxidation process on silicon surfaces was first demonstrated by Dagata et al. [26]. Since then, it has been shown that a conducting AFM tip under electrical bias could oxidize silicon as well [20,110], and that method could oxidize metal films such as Ti [116], Al [96], and Nb [107]. In this process, exposing the H-passivated surface (formed by immersion in diluted HF) to a negatively biased electrically conducting AFM tip in air generates a high local electric field which strips the hydride layer and anodically oxidizes the surface in the vicinity of the tip. The local oxide patterns, typically only a few monolayers thick and as narrow as 10 nm, can mask etches which attack the substrate material but not its oxides. The use of an AFM was also shown to be useful for the fabrication of compound semi-conductor nanoscale structure [82], devices [81,82,97,109] and metal base single-electron devices [70,98]. Single electron transistors (SETs), which are based on the principle of the Coulomb blockade phenomena, control the transfer of individual electrons in and out of an island of charge that is just tens of nanometers on a side. The AFM nanooxidation process was also applied to the fabrication of lateral metal/insulator/metal (MIM) diodes, and the MIM diodes clearly show the rectifier characteristics [106].

4.2. Application to biological sciences

The ability of AFM to measure forces in the nanoNewton range under physiological conditions makes it a very attractive tool for studying many biological

applications such as drug/protein interactions, protein/protein interaction, cell/cell or cell/protein interactions and many other largely intermolecular forces governed phenomena. Specifically, the quantification of these molecular interactions in biological systems is of interest to many researchers and engineers. A molecular level understanding of the interfacial adhesion is a necessary part of unraveling these phenomena and would be of tremendous potential benefit in associated applications such as rational drug design [61,117], molecular electronics [40], biomaterials development [85], or biosensor design. Based on the AFM's ability to generate topographical images, the AFM has evolved into a useful tool for probing single-molecules. High lateral resolution (<1 Å) and the ability to detect very low forces (~10 pN), along with the ability to operate under aqueous or physiological conditions makes it a good technique for studying biological systems. In single-molecule force spectroscopy (SMFS) experiments, individual polymers are stretched and forced through conformational transitions in order to reveal unique material properties. While SMFS experiments have been widely used to mechanically probe DNA [15,45,60,108,114], polysaccharides [63,66,90,91], proteins [60,91], and other polymers [84], very few studies have examined the mechanical properties of biopolymers on a cellular surface [19,33]. In addition, it is only recently that SMFS techniques have been used to provide quantitative *chemical* information [66,67]. Individual molecules at a cell surface mediate many important aspects of cellular phenomena such as adhesion, fusion and chemotaxis.

Although a large body of data has been gathered on the structure and function of cell membrane constituents, much of the information available on molecular mechanisms results from indirect observations. Fortunately, the NC-AFM can measure the topography, surface forces, and mechanical properties of a surface at the nanometer scale; furthermore, the development of chemically specific probes provides a direct means for studying intermolecular forces [24,29]. Single-molecule force spectroscopy (SMFS) techniques were also pioneered by the groups of Colton and Gaub, commencing with studies of molecular recognition events between ligand–receptor couples and studies on DNA [33,60,91], polysaccharides [66,67], determination of mechanical properties of surface macromolecules on fungi and measurement of elastic response of biopolymers membrane in bacterial surfaces [19].

4.2.1. Cell movement

The dynamic events that occur on a time scale of minutes in living species (e.g. Madine–Darby Canine Kidney (MDCK) cells [100]) has been examined (see Fig. 25). During AFM imaging, these cells sometimes round up and detach from the substrate which provides a platform for non-contact mode operation of the AFM.

4.2.2. Cell–surface interactions

In the last decades, cardiac myocytes have been studied in great detail mainly by electrophysiological methods. Owing to their ability of spontaneous generation of action potentials in vitro, these systems are ideal model to study detailed mechanism of muscle contraction, starting from the spontaneous generation of action potentials.

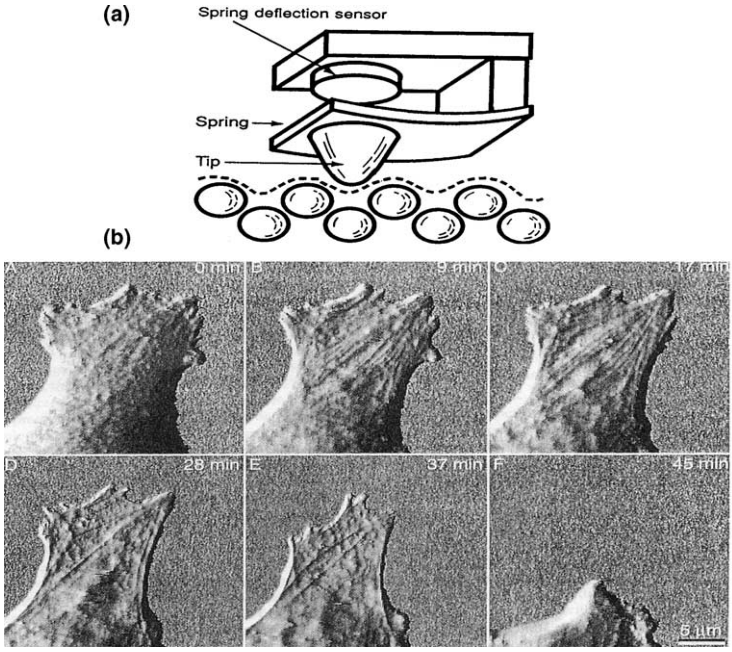

Fig. 25. (a) Atomic force microscopy and (b) time-lapse AFM series of movement in an R5 cell (derived from canine kidney epithelial cells), [100].

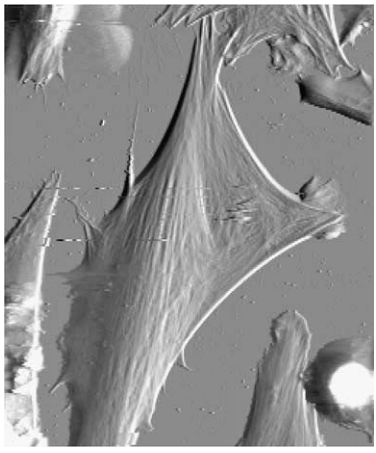

Fig. 26. AFM image of living cardiomyocytes [16,28].

The AFM has been used to analyze the contractile behavior of active single-cells as well as cells in a confluent layer, see Fig. 26, [16,28]. Using NC-AFM, the adherent single-cells can be imaged characterize the pulsing behavior of single-cells laterally.

4.2.3. Force measurement between single-molecules

Interaction forces between single-strands of DNA have been measured with the AFM by a procedure in which DNA oligonucleotides were covalently attached to a spherical probe and surface, see Fig. 27, [60]. The intrachain interaction resulting from the molecule's elasticity will manifest itself as a long-range cohesive force. Force microscopy has been applied in many biological areas, such as antigen-antibody pairs, protein-ligand interactions, protein-membrane interactions, and protein-cell interactions. A detailed review of these applications can be found in a few excellent reviews available elsewhere, [23,59,62].

4.2.4. Characterization of biomolecular assemblies and interactions

AFM's have been used for more than a decade now for numerous biological investigations such as characterizing the properties of protein-protein and protein-nucleic acid complexes, determining stoichiometries and association constants of multi-protein assemblies, observation of dynamic properties of biomolecular complexes, and measurement of intermolecular forces between biomolecules, [124].

4.2.5. Characterization of DNA–protein assemblies

The intracellular regulation of gene metabolism involves many proteins, which can bind to regulatory sites on DNA specifically and to other sites non-specifically. Searching for target sites among the vast amount of non-specific sites by these proteins is critical for gene regulation, [13,30]. Large conformational changes in both proteins and DNA can occur when proteins bind to DNA or exchange between specific sites and non-specific sites. AFM provides a straightforward method to investigate the conformations of DNA–protein assemblies because the topographic difference between proteins and DNA is obvious in an AFM image. Conformations of DNA–protein assemblies can be quantitatively distinguished by the DNA bend

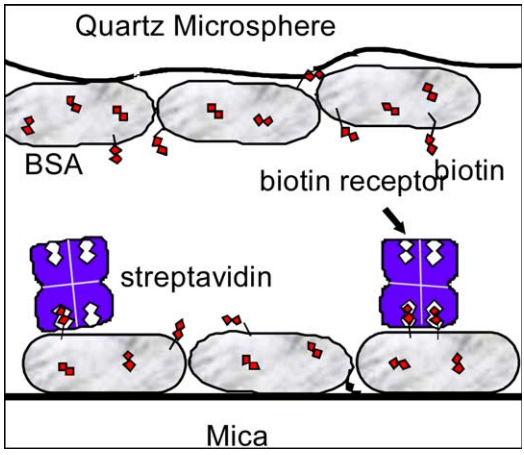

Fig. 27. AFM measurement of forces between single-molecules, [60].

angle induced by protein binding. Erie et al. [30] analyzed the fundamental roles of protein-induced DNA bending at specific sites and at non-specific sites. DNA bending induced by many other DNA binding proteins has been observed by AFM [2,48,120]. In comparison with other tools, AFM provides the spatial distribution of bending along the DNA and dynamic bending histograms of DNA–protein assemblies bound at the same location; that is, the full distribution of angles is observed. In addition to DNA bending, other quantitative information can be obtained using AFM topographic analysis, such as, a reduced DNA contour length induced by the binding of *E. coli* RNAP holoenzyme, which led to the proposal that DNA wraps around RNAP in the open promoter complex, [92]. Other examples include the characterization of the sequence specificity of S1and mung bean endonucleases by analyzing the distribution of the lengths of the digested DNA [119] and monitoring the change in the specificity of *trp* repressor with the change of enzyme concentrations, [65].

4.2.6. Following biological processes in solution imaging

The biomolecular assemblies and interactions in biological pathways take place in a timed fashion in the cell. Time-lapse AFM in solution can be used to follow these processes under near-physiological conditions. For example, the DNA-directed synthesis of RNA by *E. coli* RNAP has been observed using AFM solution imaging, [8]. In addition, the degradation of DNA by the nuclease DNase I was followed by oscillating mode AFM in solution in the presence of nickel ions, [14]. Many quantitative dynamic properties of these processes can be obtained using time-lapse AFM in solution. For example, the rate of the diffusion of *E. coli* RNAP on DNA was measured using time-lapse AFM. The rate was found to be 1.5 nucleotide/s, which is about three times slower than the speed in solution, as expected because the surface hampers the translocation, [42]. In addition to the above quantitative assays, it is also possible to qualitatively but directly correlate structural conformations and functional states of individual biomolecular assemblies using real-time AFM, [113]. For example, the conformational change of nuclear pore complexes modulated by ATP, calcium, and carbon dioxide have been studied using time-lapse AFM, [80,88,112]. These studies disclosed that ATP and calcium induce pore contraction and facilitate the transportation of macromolecules between the nucleolus and the cytosol, but carbon dioxide induces pore collapse and functions to isolate the nucleus.

4.2.7. Recent developments in biological AFM

Since the invention of AFM, many developments to increase its resolution have been made. It is well established now that in addition to instrumental factors, major factors that can affect the quality of the image include shape of the tip–sample interactions, stable immobilization of the sample on the surface, and both pH and ionic strength of the buffer used for absorbing and scanning the sample, [43,72–74].

4.2.8. Cryo-AFM

This technique holds the promise for imaging a large variety of biological samples at high resolution comparable to Electron Microscopy, [104,105]. It has been shown that the mechanical rigidity of biological materials is significantly stronger at cryogenic temperatures. The estimated Young's modulus of protein and DNA is between 10^3 and 10^4 times of that at room temperature dramatically reducing the deformation by the scanning tip. With decreased thermal motion and increased rigidity of the samples, high-resolution 3D images were demonstrated by cryo-AFM, [69]. Some images from cryo-AFM also revealed information that was not obvious in electron micrographs. For structural studies of large flexible complexes, cryo-AFM will be a very effective alternative, capable of providing information that could be elusive to other techniques.

4.2.9. Carbon nanotube probes

AFM probes are extremely essential to high-resolution, reproducible imaging of biological samples. The widely used micro-fabricated Si and Si_3N_4 AFM probes have several disadvantages, such as large radii of curvature compared to the biological sample size and brittleness. The high-resolution imaging of membrane proteins achieved using micro-fabricated probes was attributed to the small protrusions at the end of the tips. These small protrusions are not consistent from probe to probe. Carbon nanotube probes are the most promising candidates for the next generation of ultrasharp AFM probes. Their small radii (0.7–5 nm for single-walled nanotubes), high aspect ratio, extremely large Young's modulus (stiffness), and ability to be elastically buckled under large load make them ideal candidates for use as AFM probes.

4.2.10. Magnetic mode (MAC) and photothermal mode (PMOD) AFM

An intrinsic problem in the instrument is that a piezoelectric transducer vibrates the AFM probe indirectly by oscillating the probe holder. This leads to the masking of the resonance peak of the cantilever by the vibrations from the probe holder and the fluid body. In the past several years, MAC and PMOD have been used to directly vibrate the cantilever and increase the reliability of imaging in liquids. MAC uses a cantilever that has a magnetic particle attached to it or that has magnetic coating, and the cantilever is driven directly by a magnetic field. In PMOD, a bimetallic cantilever is oscillated by a pulsed diode laser. Due to the difference in the thermal expansion coefficients of the two layers, the cantilever bends and vibrates in response to the pulsed laser. Both MAC and PMOD have demonstrated high-resolution imaging capability on biological samples, [44,89].

5. Concluding remarks

The AFM imaging system can significantly impact many fabrication and manufacturing processes at molecular and nanoscale levels due to its tremendous surface microscopic capabilities such as 3D topography of nanoparticles fabrication,

metrology for MEMS, analysis of microscopic phase distribution in polymers, thin film mechanical and physical property characterization, imaging magnetic domains on digital storage media, imaging of submicron phases in metals, and defect imaging in failure analysis. These measurements can be used to quantify the texture uniformity and the relative roughness. Moreover, non-contact imaging at low tip oscillation amplitudes allows extremely high resolution imaging without tip damage. Countless biological applications such as DNA replication, protein synthesis, drug interaction, and many others are largely governed by intermolecular forces, and AFM has the ability to measure forces in the nanoNewton range. Although other techniques such as molecular forceps are able to detect forces of this magnitude, AFM is unique in the sense that it allows the user to modify and manipulate objects at the nanoscale in addition to measure the interaction forces. In addition to force quantification, AFM allows to quantify electrical surface charge. Moreover, AFM can observe the elasticity and, in fact, the viscosities of samples ranging from live cells and membranes to bone and cartilage.

References

[1] Albrecht TR, Grutter P, Horne D, Rugar D. Frequency modulation detection using high-Q cantilevers for enhanced force microscope sensitivity. J Appl Phys 1991;69:668.
[2] Allan BW, Garcia R, Maegley K, Mort J, Wong D, Lindstrom W, et al. DNA bending by EcoRI DNA methyltransferase accelerates base flipping but compromises specificity. J Biol Chem 1999;274:19269–75.
[3] Amelio S, Goldade AV, Rabe U, Scherer V, Bhushan B, Arnold W. Measurements of elastic properties of ultra-thin diamond-like carbon coatings using atomic force acoustic microscopy. Thin Solid Films 2001;392(1):75–84.
[4] Anczykowski B, Cleveland JP, Kruger D, Elings VB, Fuchs H. Analysis of the interactionmechanisms in dynamicmode SFM by means of experimental data and computer simulation. Appl Phys A 1998;66(7):S885.
[5] Anczykowski B, Gotsmann B, Fuchs H, Cleveland JP, Elings VB. How to measure energy dissipation in dynamic mode atomic force microscopy. Appl Surf Sci 1999;140:376–82.
[6] Anczykowski B, Krüger D, Fuchs H. Cantilever dynamics in quasi non-contact force microscopy: spectroscopic aspects. Phys Rev B 1996;53:15485–8.
[7] Anczykowski B, Kruger D, Babcock KL, Fuchs H. Basic properties of dynamic force spectroscopy with the scanning force microscope in experiment and simulation. Ultramicroscopy 1996;66:251–9.
[8] Argaman M, Golan R, Thomson NH, Hansma HG. Phase imaging of moving DNA molecules and DNA molecules replicated in the atomic force microscope. Nucl Acids Res 1997;25:4379–84.
[9] Ashhab M, Salapaka MV, Dahleh M, Mezic I. Dynamical analysis and control of microcantilevers. Automatica 1999;35(10):1663–70.
[10] Ashhab M, Salapaka MV, Dahleh M, Mezic I. Melnikov-based dynamical analysis of microcantilevers in scanning probe microscopy. Nonlinear Dyn 1999;20(3):197–220.
[11] Banks HT, Inman DJ. On damping mechanisms in beams. ASME J Appl Mech 1991;58:716–23.
[12] Basso M, Giarre L, Dahleh M, Mezic I. Numerical analysis of complex dynamics in atomic force microscopes. Proc IEEE Conf Control Appl. Trieste, Italy, September 1998, pp. 1026–1030.
[13] Berg OG, Winter RB, von Hippel PH. Diffusion-driven mechanisms of protein translocation on nucleic acids. 1. Models and theory. Biochemistry 1981;20:6929–48.
[14] Bezanilla M, Drake B, Nudler E, Kashlev M, Hansma PK, Hansma HG. Motion and enzymatic degradation of DNA in the atomic force microscope. Biophys J 1994;67:2454–9.

[15] Boland T, Ratner BD. Direct measurement of hydrogen bonding in dna nucleotide bases by atomic force microscopy. Proc Nat Acad Sci USA 1995;92:5297.
[16] Braet F, Rotsch C, Wisse E, Radmacher M. Comparison of fixed and living liver endothelial cells by atomic force microscopy. Appl Phys A 1997;66(7):S575–8.
[17] Burnham NA, Colton RJ. Measuring the nanomechanical properties and surface forces of materials using an atomic force microscope. J Vacuum Sci Technol A 1989;7:2906.
[18] Burnham NA, Behrend OP, Oulevey F, Gremaud G, Gallo PJ, Gourdon D, et al. How does a tip tap? Nanotechnology 1997;8(2):67–75.
[19] Camesano TA, Wilkinson KJ. Single molecule study of xanthan conformation using atomic force microscopy. Biomacromolecules 2001;2:1184–91.
[20] Campbell PM, Snow ES, McMarr PJ. AFM-based fabrication of Si nanostructures. Phys B: Condens Matter 1996;227(1–4):315–7.
[21] Chen J, Workman RK, Sarid D, Hooper R. Numerical simulations of a scanning force microscope with a large-amplitude vibrating cantilever. Nanotechnology 1994;5:199–204.
[22] Chen X, McGurk SL, Davies MC, Roberts CJ, Shakesheff KM, Tendler SJB, et al. Chemical and morphological analysis of surface enrichment in a biodegradable polymer blend by phase-detection imaging atomic force microscopy. Macromolecules 1998;31:2278.
[23] Clausen-Schaumann H, Seitz M, Krautbauer R, Gaub HE. Force spectroscopy with single bio-molecules. Curr Opin Chem Biol 2000;4:524–30.
[24] Colton RJ, Baselt DR, Dufrene YF, Green JBD, Lee GU. Scanning probe microscopy. Curr Opin Chem Biol 1997;1:370–7.
[25] Dadfarnia M, Jalili N, Xian B, Dawson DM. A Lyapunov-based piezoelectric controller for flexible cartesian robot manipulators. ASME J Dyn Syst, Measurements and Control 2004;126:xx–xx+13.
[26] Dagata JA, Schneir J, Harary HH, Evans CJ, Postek MT, Bennett J. Modification of hydrogen-passivated silicon by a scanning tunneling microscope operating in air. Appl Phys Lett 1990;56:2001.
[27] DeVecchio D, Bhushan B. Localized surface elasticity measurements using an atomic force microscope. Rev Scientific Instrum 1997;68(12):4498–505.
[28] Domke J, Parak WJ, George M, Gaub HE, Radmacher M. Mapping the mechanical pulse of single cardiomyocytes with the atomic force microscope. European Biophys J 1999;28(3):179–86.
[29] Dufrêne YF, Boland T, Schneider JS, Barger WR, Lee GU. Characterization of the physical properties of model biomembranes at the nanometer scale with the atomic force microscope. Faraday Discuss 1998;111:79–94.
[30] Erie DA, Yang G, Schultz HC, Bustamante C. DNA bending by Cro protein in specific and nonspecific complexes: implications for protein site recognition and specificity. Science 1994;266:1562–6.
[31] Fang Y, Dawson D, Feemster M, Jalili N. Active interaction force identification for atomic force microscope applications: lumped model. Proc 2002 Int Mech Eng Congr Exposition (IMECE'02). New Orleans, Louisiana (November 2002).
[32] Fang Y, Feemster M, Dawson D, Jalili N. Active interaction force identification for atomic force microscope applications: PDE model. Proc 41st IEEE Conf Decision Control (CDC'02). Las Vegas, Nevada (December 2002).
[33] Florin EL, Moy VT, Gaub HE. Adhesive forces between individual ligand–receptor pairs. Science 1994;264:415–7.
[34] Fung R, Huang S. Dynamic modeling and vibration force microscope. ASME J Vib Acoust 2001;123:502–9.
[35] Gahlin R, Jacobson S. Novel method to map and quantify wear on a micro-scale. Wear 1998;222(2):93–102.
[36] Giessibl FJ. Atomic resolution of the Silicon (1 1 1)-(7 × 7) surface by atomic force microscopy. Science 1995;267(5194):68.
[37] Goeken M, Kempf M. Microstructural properties of superalloys investigated by nanoindentations in an atomic force microscope. Acta Mater 1999;47(3):1043–52.
[38] Göken M, Vehoff H, Neumann P. Atomic force microscopy investigations of loaded crack tips in NiAl. J Vacuum Sci Technol B 1996;14:1157–61.

[39] Göken M, Vehoff H, Neumann P. Investigation of loaded crack tips in NiAl by atomic force microscopy. Scrip Metall Mater 1995;33:1187–92.
[40] Goldhabergordon D, Montemerlo MS, Love JC, Opiteck GJ, Ellenbogen JC. Overview of nanoelectronic devices. Proc IEEE 1997;85:521–40.
[41] Güthner P. Simultaneous imaging of Si(1 1 1) 7×7 with atomic resolution in scanning tunneling microscopy, atomic force microscopy, and atomic force microscopy non-contact mode. J Vacuum Sci Technol B 1996;14:2428.
[42] Guthold M, Zhu X, Rivetti C, Yang G, Thomson NH, Kasas S, et al. Direct observation of one-dimensional diffusion and transcription by escherichia coli RNA polymerase. Biophys J 1999;77:2284–94.
[43] Hafner JH, Cheung CL, Woolley AT, Lieber CM. Structural and functional imaging with carbon nanotube AFM probes. Prog Biophys Molecular Biol 2001;77:73–110.
[44] Han W, Lindsay SM, Jing T. A magnetically driven oscillating probe microscope for operation in liquids. Appl Phys Lett 1996;69:4111–4.
[45] Hansma HG et al. Recent advances in atomic force microscopy of DNA. Scanning 1993;15:296–9.
[46] Heaton MG, Prater CB, Kjoller KJ. Lateral and chemical force microscopy: mapping surface friction. Digital Instruments.
[47] Hsu S, Fu L. Robust output high-gain feedback controllers for the atomic force microscope under high data sampling rate. Proc IEEE Int Conf Control Appl. Kohala Coast-Island HI, August 1999, pp. 1626–1631.
[48] Hun Seong G, Kobatake E, Miura K, Nakazawa A, Aizawa M. Direct atomic force microscopy visualization of integration host factor-induced DNA bending structure of the promoter regulatory region on the pseudomonas TOL plasmid. Biochem Biophys Res Commun 2002;291:361–6.
[49] Hutter JL, Bechhoefer J. Calibration of atomic-force microscope tips. Rev Scientific Instrum 1993;64(7):1868–73.
[50] Israelachvili JN. Intermolecular and surface forces. Boston, MA: Academic Press; 1985.
[51] Itoh T, Kataoka K, Suga T. Characteristics of low force contact process for MEMS probe cards. Sensors and Actuators, A: Physical 97–98:462–467.
[52] Tamayo J, Humphris ADL, Owen RJ, Miles MJ. High-Q dynamic force microscopy in liquid and its application to living cells. Biophys J 2001;81:526–37.
[53] Jalili N, Dadfarnia M, Dawson DM. A fresh insight into the microcantilever–sample interaction problem in non-contact atomic force microscopy. ASME J Dyn Syst Measurements Control 2004;126:XX–XX+9.
[54] Jalili N, Dadfarnia M, Dawson DM. Distributed-parameters base modeling and vibration analysis of micro-cantilevers used in atomic force microscopy. Proc 19th ASME Biennial Conf Mech Vib Noise, Symp Dyn Vibration Robotic Syst. Chicago, Illinois (September 2003).
[55] Junno T, Carlsson SB, Xu H, Montelius L, Samuelson L. Fabrication of quantum devices by angstrom-level manipulation of nanoparticles with an atomic force microscope. Appl Phys Lett 1998;72(5):548.
[56] Kaneko R, Miyamoto T, Andoh Y, Hamada E. Microwear. Thin Solid Films 1996;273(1–2):105–11.
[57] Kempf M, Göken M, Vehoff H. Nanohardness measurements for studying local mechanical properties of metals. Appl Phys A: Mater Sci Process 1998;66:S843–6.
[58] Laxminarayana K, Jalili N. A review of modeling and operational modes of atomic force microscopy systems with application to molecular manufacturing. Proc 2003 ASME Int Mech Eng Congr Exposition, Symp. Nanoscale Dyn. Sensing Control. Washington DC (November 2003).
[59] Leckband D. Measuring the forces that control protein interactions. Ann Rev Biophys Biomol Struct 2000;29:126.
[60] Lee GU, Chrisey LA, Colton RJ. Direct Measurement of the forces between complementary strands of DNA. Science 1994;266:771–3.
[61] Lewis RA, Leach AR. Current methods for site-directed structure generation. J Computer-Aided Mol Des 1994;8:467–75.
[62] Luckham PF, Smith K. Direct measurement of recognition forces between proteins and membrane receptors. Faraday Discuss 1999;111:307–20.

[63] Ludwig M, Rief M, Schmidt L, Li H, Oesterhelt F, Gautel M, et al. AFM—a tool for single molecule experiments. Appl Phys A: Mater Sci Process 1999;68:173–6.
[64] Magonov SN, Elings VB, Whangbo MH. Phase imaging and stiffness in tapping-mode atomic force microscopy. Surf Sci 1997;375:1385–91.
[65] Margeat E, Le Grimellec C, Royer CA. Visualization of *trp* repressor and its complexes with DNA by atomic force microscopy. Biophys J 1998;75:2712–20.
[66] Marszalek PE, Oberhauser AF, Pang YP, Fernandez JM. Polysaccharide elasticity governed by chair–boat transitions of the glucopyranose ring. Nature 1998;396:661.
[67] Marszalek PE, Pang YP, Li H, El Yazal J, Oberhauser AF, Fernandez JM. Atomic levers control pyranose ring conformation. Proc Nat Acad Sci USA 1999;96:7894–8.
[68] Martin Y, Williams CC, Wikramasinghe HK. Atomic force microscope-force mapping and profiling on a Sub 100-A§ scale. J Appl Phys 1987;61:4723.
[69] Mat-Arip Y, Garver K, Chen C, Sheng S, Shao Z, Guo P. Three-dimensional Interaction of Phi29 pRNA dimer probed by chemical modification interference, Cryo-AFM, and cross-linking. J Biol Chem 2001;276:32575–84.
[70] Matsumoto K, Ishii M, Segawa K, Oka Y, Vartanian BJ, Harris JS. Room temperature operation of a single electron transistor made by the scanning tunneling microscope nanooxidation process for the TiO_x/Ti system. Appl Phys Lett 1996;68(1):34.
[71] Miyahara K, Nagashima N, Ohmura T, Matsuoka S. Evaluation of mechanical properties in nanometer scale using AFM-based nanoindentation tester. Nanostruct Mater 1999;12(5).
[72] Mou J, Czajkowsky DM, Zhang Y, Shao Z. High-resolution atomic-force microscopy of DNA: the pitch of the double helix. FEBS Lett 1995;371:279–82.
[73] Muller DJ, Engel A. The height of biomolecules measured with the atomic force microscope depends on electrostatic interactions. Biophys J 1997;73:1633–44.
[74] Muller DJ, Fotiadis D, Scheuring S, Muller SA, Engel A. Electrostatically balanced subnanometer imaging of biological specimens by atomic force microscope. Biophys J 1999;76:1101–11.
[75] Nagashima N, Matsuoka S, Miyahara K. Nanoscopic hardness measurement by atomic force microscope. JSME Int J, Series A: Mech Mater Eng 1996;39(3):456–62.
[76] Nagel LW. SPICE2: a computer program to simulate semiconductor circuits. University of California, Berkeley, Tech. Rep. Memo ERLM520, 1975.
[77] Niedermann Ph, Hänni W, Blanc N, Christoph R, Burger J. Chemical vapor deposition diamond for tips in nanoprobe experiments. J Vacuum Sci Technol A 1996;14:1233.
[78] Niedermann Ph, Hänni W, Morel D, Perret A, Skinner N, Indermühle PF, et al. CVD diamond probes for nanotechnology. Appl Phys A 1998;66:S31–4.
[79] Niedermann Ph, Hänni W, Thurre S, Gjoni M, Perret A, Skinner N, et al. Mounting of micromachined diamond tips and cantilevers. Surf Interf Anal 1999;27:296–8.
[80] Oberleithner H, Schillers H, Wilhelmi M, Butzke D, Danker T. Nuclear pores collapse in response to CO_2 imaged with atomic force microscopy. Pflugers Arch European J Physiol 2000;439:251–5.
[81] Okada Y, Amano S, Iuchi Y, Kawabe M, Harris JS. AlGaAs/GaAs tunneling diode integrated with nanometer-scale oxides patterned by atomic force microscope. Electron Lett 1998;34(12): 1262–3.
[82] Okada Y, Amano S, Kawabe M, Shimbo BN, Harris JS. Nanoscale oxidation of GaAs-based semiconductors using atomic force microscope. J Appl Phys 1998;83(4):1844–7.
[83] Olbrich A, Ebersberger B, Boit C, Niedermann P, Hänni W, Vancea J, et al. High aspect ratio all diamond tips formed by focused ion beam for conducting atomic force microscopy. J Vacuum Sci Technol B 1999;17(4):1570–4.
[84] Ortiz C, Hadziioannou G. Entropic elasticity of single polymer chains of Poly (methylacrylic acid) measured by atomic force microscopy. Macromolecules 1999;32:780–7.
[85] Peppas NA, Langer R. New challenges in biomaterials. Science 1994;263:1715–20.
[86] Pickering JP, Vancso GJ. Apparent contrast reversal in tapping mode atomic force microscope images on films of polystyrene-b-polyisoprene-b-polystyrene. Polym Bull 1998;40:549–54.
[87] Prater CB, Strausser YE. TappingMode™ atomic force microscopy—applications to semiconductors. Digital Instruments, Veeco Metrology Group.

[88] Rakowska A, Danker T, Schneider SC, Oberleithner H. ATP-induced shape change of nuclear pores visualized with the atomic force microscope. J Membrane Biol 1998;163(2):129–36.
[89] Ratcliff GC, Erie DA, Superfine R. Photothermal modulation for oscillating mode atomic force microscopy in solution. Appl Phys Lett 1998;72:1911–3.
[90] Rief M, Fernandez JM, Gaub HE. Elastically coupled two-level systems as a model for biopolymer elasticity. Phys Rev Lett 1998;81:4764–7.
[91] Rief M, Gautel M, Oesterhelt F, Fernandez JM, Gaub HE. Reversible unfolding of individual tin immunoglobulin domains by AFM. Science 1997;276:1109–12.
[92] Rivetti C, Guthold M, Bustamante C. Wrapping of DNA around the *E. coli* RNA polymerase open promoter complex. EMBO J 1999;18:4464–75.
[93] Sahin O, Atalar A. Analysis of tip–sample interaction in tapping-mode atomic force microscope using an electrical circuit simulator. Appl Phys Lett 2001;78(19):2973–5.
[94] Salapaka MV, Bergh HS, Lai J, Majumdar A, McFarland E. Multimode noise analysis of cantilevers for scanning probe microscopy. J Appl Phys 1997;81(6):2480–7.
[95] Salapaka M, Chen D. Stability and sensitivity analysis of periodic orbits in tapping mode atomic force microscopy. Proc Conf Decision Control. Tampa FL, December 1998, pp. 2047–2052.
[96] Sasa S, Ikeda T, Akahori M, Kajiuchi A, Inoue M. Novel nanofabrication process for InAs/AlGaSb heterostructures utilizing atomic force microscope oxidation. Japanese J Appl Phys, Part 1: Regular Papers and Short Notes and Review Papers 1999;38(2B):1064–6.
[97] Sasa S, Ikeda T, Dohno C, Inoue M. Atomic force microscope nanofabrication of InAs/AlGaSb heterostructures. Japanese J Appl Phys, Part 1: Regular Papers and Short Notes and Review Papers 1997;36(6B):4065–7.
[98] Sasa S, Yodogawa S, Ohya S, Inoue M. A single-electron transistor produced by nanoscale oxidation of InAs. Japanese J Appl Phys, Part 1: Regular Papers and Short Notes and Review Papers 2001;40(3B):2026–8.
[99] Scherer V, Bhushan B, Rabe U, Arnold W. Local elasticity and lubrication measurements using atomic force and friction force microscopy at ultrasonic frequencies. IEEE Trans Mag 1997;33(5):4077–9.
[100] Schoenenberger CA, Hoh J. Immuno-atomic force microscopy of purple membrane. Biophys J 1996;70(4):1796.
[101] Sebastian A, Salapaka M, Chen D, Cleveland J. Harmonic analysis based modeling of tapping-mode AFM. Proc Am Control Conf. San Diego CA, June 1999, pp. 232–236.
[102] Serry FM, Strausser EYE, Magonov J, Thornton SJ, Ge L. Surface characterization using atomic force microscopy. Surf Eng 1999;15(4):285–90.
[103] Serry FM, Kjoller K, Thornton JT, Tench RJ, Cook D. Electric force microscopy, surface potential imaging, and surface electric modification. Digital Instruments, 1999.
[104] Shao Z, Shi D, Somlyo AV. Cryoatomic force microscopy of filamentous actin. Biophys J 2000;78:950–8.
[105] Shao Z, Zhang Y. Biological cryo atomic force microscopy: a brief review. Ultramicroscopy 1996;66:141–52.
[106] Shirakashi JI, Matsumoto K, Miura N, Konagai M, Konagai M. Single-electron charging effects in Nb/Nb oxide-based single-electron transistors at room temperature. Appl Phys Lett 1998;72(15):1893.
[107] Shirakashi JI, Matsumoto K, Miura N, Konagai M. Single-electron transistors (SETs) with Nb/Nb oxide system fabricated by atomic force microscope (AFM) nano-oxidation process. Japanese J Appl Phys, Part 2: Lett 1997;36(9):1257–60.
[108] Smith SB, Cui Y, Bustamante C. Overstretching B-DNA: the elastic response of individual double-stranded and single-stranded DNA molecules. Science 1996;271:795–9.
[109] Snow ES, Campbell PM. AFM fabrication of sub-10-nanometer metal–oxide devices with in situ control of electrical properties. Science 1995;270(5242):1639.
[110] Snow ES, Campbell PM. Fabrication of Si nanostructures with an atomic force microscope. Appl Phys Lett 1994;64(15):1932.

[111] Spatz JP, Sheiko S, Möller M, Winkler RG, Reineker R, Marti O. Forces affecting the substrate in resonant tapping force microscopy. Nanotechnology 1995;6:40–4.
[112] Stoffler D, Goldie KN, Feja B, Aebi U. Calcium-mediated structural changes of native nuclear pore complexes monitored by time-lapse atomic force microscopy. J Molecular Biol 1999;287:741–52.
[113] Stolz M, Stoffler D, Aebi U, Goldsbury C. Monitoring biomolecular interactions by time-lapse atomic force microscopy. J Struct Biol 2000;131:171–80.
[114] Strick TR, Allemand JF, Bensimon D, Bensimon A, Croquette V. The elasticity of single supercoiled DNA molecule. Science 1996;271:1835–7.
[115] Sugawara Y, Ueyama H, Uchihashi T, Ohta M, Morita S, Suzuki M, et al. True atomic resolution imaging with non-contact atomic force microscopy. Appl Surf Sci 1997;113/114:364–70.
[116] Sugimura H, Uchida T, Kitamura N, Masuhara H. Scanning tunneling microscope tip-induced anodization of titanium: characterization of the modified surface and application to the metal resist process for nanolithography. J Vacuum Sci Technol B: Microelectron Nanometer Struct 12(5):2884–2888.
[117] Sun E, Cohen FE. Computer-assisted drug discovery—a review. Gene 1993;137:127–32.
[118] Sundararajan S, Bhushan B. Development of a continuous microscratch technique in an atomic force microscope and its application to study scratch resistance of ultrathin hard amorphous carbon coatings. J Mater Res 2001;16(2):437–45.
[119] Umemura K, Nagami F, Okada T, Kuroda R. AFM characterization of single strand-specific endonuclease activity on linear DNA. Nucl Acids Res 2000;28(9):E39.
[120] van Noort J, Orsini F, Eker A, Wyman C, de Grooth B, Greve J. DNA bending by photolyase in specific and non-specific complexes studied by atomic force microscopy. Nucl Acids Res 1999;27:3875–80.
[121] Westra KL, Thomson DJ. Microstructure of thin films observed using atomic force microscopy. Thin Solid Films 1995;257(1):15–21.
[122] Wiesendanger R. Scanning probe microscopy and spectroscopy. Great Britain: Cambridge University Press; 1994.
[123] Yamamoto A, Watanabe A, Tsubakino H, Fukumoto S. AFM observations of microstructures of deposited magnesium on magnesium alloys. Mater Sci Forum 2000;350:241–6.
[124] Yong Y, Hong W, Erie DA. Quantitative characterization of biomolecular assemblies and interactions using atomic force microscopy. Methods 2003;29:175–87.